ELSEVIER

Contents lists available at ScienceDirect

International Journal of Biological Macromolecules

journal homepage: www.elsevier.com/locate/ijbiomac



Check for updates

Tunable microphase-regulated silk fibroin/poly (lactic acid) biocomposite materials generated from ionic liquids

Qianqian Deng^{a,b}, Fang Wang^{a,b,*}, Christopher R. Gough^c, Xiao Hu^{c,d,e,**}

- a Center of Analysis and Testing, Nanjing Normal University, Nanjing 210023, China
- ^b School of Chemistry and Materials Science, Nanjing Normal University, Nanjing 210023, China
- ^c Department of Physics and Astronomy, Rowan University, Glassboro, NJ 08028, USA
- ^d Department of Biomedical Engineering, Rowan University, Glassboro, NJ 08028, USA
- e Department of Molecular and Cellular Biosciences, Rowan University, Glassboro, NJ 08028, USA

ARTICLE INFO

Keywords: Silk Poly(D,L-lactic acid) Ionic liquid Composite materials Biomedical applications

ABSTRACT

One of the most effective and promising strategies to develop novel biomaterials with unique, tunable structure and physicochemical properties is by creating composite materials that combine synthetic polymers with natural proteins using ionic liquids. In this study, biodegradable poly(p,L-lactic acid) (PDLLA) was blended with silk fibroin (SF) to create biocompatible films using an ionic liquid-based binary solvent system (1-butyl-3-methylimidazolium chloride/N,N-dimethylformamide), which can maintain the molecular weights of the proteins/ polymers and encourage intermolecular interactions between the molecules. The effects of varying the ratio of PLA to SF were studied using scanning electron microscopy (SEM), Fourier transform infrared spectroscopy (FTIR), X-ray diffraction (XRD), differential scanning calorimetry (DSC), thermogravimetric analysis (TGA), water contact angle testing, and cytotoxicity analysis as well as enzymatic degradation. Results showed that the composite films were homogeneously blended on the macroscopic scale and exhibited typical fully miscible polymer blend characteristics. By increasing the SF content in the composites, the amounts of β -sheets in the films were significantly increased, allowing for SF to act as a physical crosslinker to maintain the stability of the protein-polymer network. Additionally, SF significantly improved the hydrophilicity and biocompatibility of the material and promoted the self-assembly of micelle structures in the biocomposites. Different topologies in the films also provided beneficial surface morphology for cell adhesion, growth, and proliferation. Overall, this study demonstrated an effective fabrication method for a fine-tuned polymer blends combining synthetic polymer and protein for a wide variety of biomedical and green material applications.

1. Introduction

There is increasing interest in the need for biocompatible materials and green chemistry, leading to the widespread attention on innovative biodegradable natural polymers [1–14]. One natural polymer that attracts much attention is silk fibroin (SF) fibers spun from arthropods. SF fibers are low cost, non-toxic, and biodegradable. They also show promising biocompatibility in several biomedical applications [15–23] due to minimal inflammation *in vivo* [11–14]. As a biopolymer, however, SF has limitations in its physicochemical properties which limit its applications [14–15]. To overcome this, a common practice is to blend SF with synthetic polymers to improve its material properties [8,11,14,24–25]. When blended effectively, composite materials can

utilize the strengths of the individual components of the composite to overcome the shortcomings of the other components and obtain an ideal material for unique applications [26–28].

Fabrication of materials using SF is also met with another issue: due to strong intermolecular hydrogen bonding and crystallinity provided by the β -sheet structure of SF, is can be difficult to dissolve SF into solution for biomaterial fabrication [29–30]. Typically, dissolution of SF requires strong acids (sulfuric acid, phosphoric acid) [31], high-concentration salt solutions (LiSCN aqueous solution, LiBr-H₂O solution, CaCl₂-C₂H₅OH-H₂O solution) [32–34,35], fluorinated solutions (hexafluoroisopropanol aqueous solution, trifluoroacetic acid) [31,36] or salt-acid systems (CaCl₂-FA solution) [20] to effectively dissolve SF on the molecular level. None of these solvent systems are ideal for

 $^{^*\} Correspondence\ to:\ F.\ Wang,\ Center\ of\ Analysis\ and\ Testing,\ Nanjing\ Normal\ University,\ Nanjing\ 210023,\ China.$

^{**} Correspondence to: X. Hu, Department of Physics and Astronomy, Rowan University, Glassboro, NJ 08028, USA. *E-mail addresses:* wangfang@njnu.edu.cn (F. Wang), hu@rowan.edu (X. Hu).

biomaterials or green manufacturing, as they are toxic, volatile, difficult to recycle, and result in destruction of the protein structure and molecular weight which impacts the material properties of the biomaterial [31–36]. The choice of solvent is therefore a critical element of success for the fabrication of SF biomaterials [35].

A new class of solvents that present an environmentally friendly alternative while solving many of the toxicity and degradation issues of conventional solvents is ionic liquids [37–39]. Ionic liquids contain both organic and inorganic components and are able to dissolve proteins by denaturing their secondary structure while maintaining their molecular weight and encouraging intermolecular interactions through electrostatic forces [40-42]. In addition, ionic liquids are thermally stable, electrically conductive, less toxic, and can be easily recycled [43-47]. Many current studies have already shown the potential of ionic liquids in the fabrication of composite biomaterials. For example, Park et al. [11] utilized 1-ethyl-3-methylimidazole acetate (EMIMAc) to treat cellulose and other biopolymers (bacterial cellulose, β -cyclodextrin, dextran, starch, agarose, agar, gum arabic, *j*-carrageenan, chitosan, xanthan gum, xylan, lignin, gelatin, collagen, silk) to co-dissolve both biopolymers into cellulose-based composite films. By tailoring the choice and ratio of polymers, a range of films with different material properties were produced. Tian et al. [1] used 1-butyl-3-methylimidazolium chloride salt (BMIMCI) to fabricate cellulose/SF composite films at a mass ratio of 3:1. Through their characterization, they were able to show specific molecular interactions between cellulose and SF through intermolecular bonding between the -NH group of SF and the -OH groups of C2 and C3 on cellulose. Simultaneously, the use of ionic liquid enhanced the β -sheet content introduced by SF while reducing the less ordered β -turn structures within the composite films. Through this mechanism, ionic liquid was able to improve the mechanical strength of the composite films by enhancing molecular interactions. In another feat to the environmental benefits of BMIMCl, Guiza et al. [9] dissolved chicken feather and cardboard in BMIMCl and regenerated the samples by freeze-drying to produce keratin/cellulose films with strong thermal and mechanical properties. The composite films were found to have strong adsorption capacity for oils and organic liquids coupled with good recyclability and reusability, making them promising materials for the cleanup of oil spills. While these and several other [11,48–50] studies have shown the effectiveness of ionic liquid for preparing natural polymer-based composites, there is very little work being done between proteins and aliphatic synthetic polymers using ionic liquid-based solvent systems [6-9,24-25].

In this study, we used the ionic liquid 1-butyl-3-methylimidazole (BMIMCL) and *N,N*-dimethylformamide (DMF) as a binary solvent system for the first time to obtain different ratios of silk fibroin-poly(D,L-lactic acid) (SF/PDLLA) blend films. The composites were then studied using scanning electron microscopy (SEM), Fourier transform infrared spectroscopy (FTIR), X-ray diffraction (XRD), differential scanning calorimetry (DSC), thermogravimetric analysis (TGA), water contact angle measurements, and cytotoxicity testing to analyze their morphology, structure, and thermal properties, and to evaluate their biological performance. The results in this study revealed a novel microscopic interaction mechanism between SF and PDLLA [31,51], and provide a new strategy for the comprehensive understanding of the mechanism and function in the preparation of SF-based composites by ionic liquid which expand the applications of ionic liquid in the preparation of other natural-synthetic polymer composites.

2. Experimental section

2.1. Materials

Chinese *Bombyx mori* silk cocoons were purchased from Dandong July Trading Co., Ltd. (China). Prior to use, they were degummed, washed with water, and dried to obtain regenerated silk fibroin (SF) fibers. The poly ($_{D,L}$ -lactic acid) (PDLLA, $M\eta = 10,000$) was derived from

Shenzhen Yisheng New Material Co., Ltd. (China). The ionic liquid used in this study, 1-butyl-3-methylimidazolium chloride (BMIMCl), was provided by Shanghai Chengjie Chemical Co., Ltd. (China), and *N*,*N*-dimethylformamide (DMF) of analytical grade with a purity greater than 99% was obtained from Sinopharmaceutical Chemical Reagents Co., Ltd. (China).

2.2. Preparation of SF/PDLLA composite films

The degummed SF fibers were cut into small pieces and added to the ionic liquid BMIMCl in portions. To facilitate dissolution, the fiber-BMIMCl solution was heated in 100 $^{\circ}$ C water bath for 48 h to obtain an 8 wt% clear amber SF solution. PDLLA was dissolved into N-N dimethylformamide (DMF) using a mechanical shaker to create 5 wt% PLA solutions. Following preparation of both solutions separately, the SF/BMIMCl and PDLLA/DMF solutions were mixed in various ratios (0:5, 1:5, 2:5, 3:5, 5:5, 5:3, 5:2, 5:1, 5:0) at 95 °C under reflux conditions for 7 h to obtain uniform mixed solutions of SF/PDLLA. SF/PDLLA solutions were then slowly poured into a petri dish, then vacuum freezedried for 2 days to form gels. To solidify the gel-like composites into films, the composites were immersed in ethanol until solidified. Finally, excess ionic liquid on the surface of the films was removed using a continuous deionized water rinse followed by vacuum freeze-drying. Fig. 1(I-II) shows a schematic diagram of the fabrication of the SF/ PDLLA blend films based on the ionic liquid binary solvent system.

2.3. Scanning electron microscopy (SEM)

Scanning electron microscopy (SEM, JSM-7600F, Japan JEOL company) was used to observe the morphology of SF/PDLLA composite films. Images were taken at an accelerating voltage of $10~\rm kV$ and working distance of $15~\rm mm$. Prior to imaging, films were sputter-coated in gold $3-4~\rm times$ each, for $30s~\rm each$ time, at a current of $20~\rm mA$, to improve their conductivity.

2.4. Fourier transform infrared spectroscopy (FTIR)

The molecular conformation of SF-PDLLA composite films were studied by Fourier transform infrared spectrometry (NEXUE, Nicolet, USA) with the KBr compression method. Spectrograms were obtained between 4000 and 400 $\rm cm^{-1}$ at a resolution of 4 $\rm cm^{-1}$ with 64 scans per sample.

2.5. X-ray diffractometer (XRD)

The crystallinity of the composite films was studied using X-ray diffraction. CuK α radiation, 40 kV tube pressure, and 50 mA tube current were used to obtain readings from 5° to 50° at a scanning rate of with $10^\circ/min$.

2.6. Differential scanning calorimetry (DSC)

RV differential scanning calorimeter (RVDSC, DSC7000X, Japan JEOL company) was used to study different ratios of SF/PDLLA composite films in standard DSC (DSC) mode and temperature modulated DSC (TMDSC) mode. Standard mode DSC measurements were taken from $-20~^{\circ}\text{C}$ to $400~^{\circ}\text{C}$ at a heating rate of $10~^{\circ}\text{C/min}$. In temperature-modulated DSC (TMDSC) mode, the rate of heating was 2 $^{\circ}\text{C/min}$ from $-20~^{\circ}\text{C}$ to $220~^{\circ}\text{C}$ with a modulation temperature amplitude of $3~^{\circ}\text{C}$ and frequency of 0.02~Hz. Testing was performed on dry SF/PDLLA composite films encapsulated in aluminum plates under nitrogen purge gas with a flow rate of 30~mL/min.

2.7. Thermogravimetric analysis (TGA)

Pyris 1 TGA (Perkin-Elmer, USA) was used for thermogravimetric

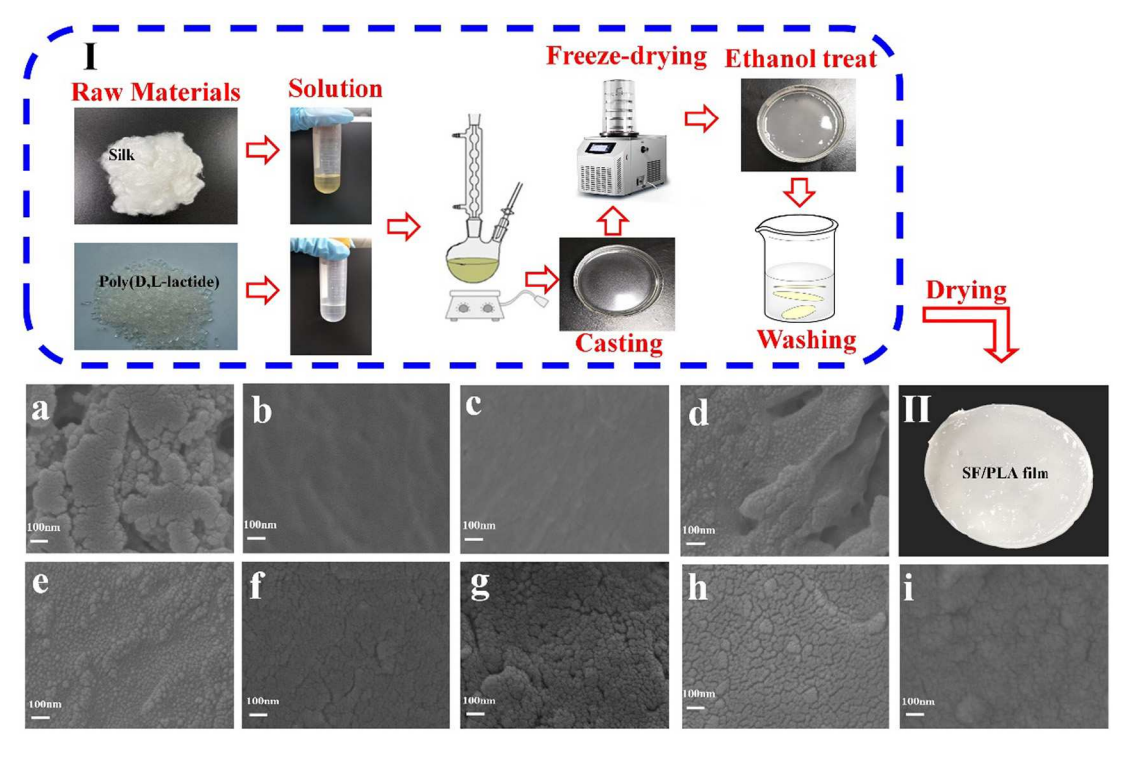


Fig. 1. (I) Schematic fabrication of SF/PDLLA blend material film based on ionic liquids. And SEM images of SF/PDLLA composite films (II) with different mass ratios: SF/PDLLA = 5/0 (a), 5/1 (b), 5/2 (c), 5/3 (d) 5/5 (e), 3/5 (f), 2/5 (g), 1/5 (h), 0/5 (i).

(TG) analysis. Samples were heated from 20 $^{\circ}C$ to 550 $^{\circ}C$ at 10 $^{\circ}C/min$ while under nitrogen purge gas with a flow rate of 50 mL/min. The change in sample mass was recorded while heating.

2.8. Water contact angle test

The hydrophilicity of SF/PDLLA composite films with different SF: PDLLA ratios was tested by using the sessile drop method. Ultrapure water was dripped onto the films using a needle, followed by photographing with an optical contact angle measuring instrument after 5 s of contact between the water and the film. The photographs were used to calculate the static contact angle. For each film, measurements were taken at least 3 times and the average value was reported.

2.9. Cytotoxicity and biocompatibility

L929 (mouse fibroblasts) cells were used to study the biocompatibility of composite materials in vitro. The biological performance of the SF/PDLLA composite films was evaluated based on the contact between cells and the films. Prior to seeding cells on the films, all films were sterilized by exposing them to UV light for 2 h and then immersing in 70% ethanol. Films were then rinsed with phosphate-buffered saline solution (PBS) three times and cell culture medium once to remove ethanol and prepare the films for the cells. The cell culture medium contained 10% fetal bovine serum at a concentration of 5 mg/mL. After 24 h of soaking, the supernatant was taken as the extraction of the composite films. The incubated L929 cells were suspended in new Dulbecco modified Eagle medium (DMEM) at a concentration of 104 cells/ cm³ with 10% (v/v) fetal bovine serum added. 200 μ L of the above culture solution was plated into 96-well plates and incubated at 37 $^{\circ}\text{C}$ in a $5\%\ CO_2$ cell incubator for $24\ h.$ The cell culture medium was then replaced with the supernatant-fetal bovine serum solution from the composite films incubated for an additional 6, 24, and 48 h. At set time points, the solution was removed and replaced with 200 µL of 0.5 mg/ mL MTT (3-[4,5-dimethylthiazole-2]-2,5-diphenyltetrazolium bromide) solution to quantify cell viability. After incubating for 4 h, the

supernatant was removed and 200 μL of DMSO was added. The solution was shaken for 10 min at room temperature to completely dissolve the formazan, and then the ultraviolet absorbance at 490 nm was measured on a BioTek immunoassay analyzer (EL-x800). Three parallel experiments were taken for each sample and the average absorbance was recorded and compared to a control group with only cells and no material from the films. The following equation was used to quantify cell viability:

$$Viability = \frac{D_s}{D_c} \times 100\%$$

where D_s is the absorbance of the cell culture solution exposed to the films, D_c is the absorbance of the control solution.

2.10. Enzyme degradation

About 10 mg of SF/PDLLA composite films (SP5-0, SP5-2, SP5-5 and SP3-5) were weighed and immersed into a 10 mL PBS solution (pH 7.4) containing 3.1 U/mL of chymotrypsin (McLean, China) at 37 $^{\circ}\text{C}$ for 24 h. After enzymatic degradation, the remaining films were taken out, rinsed gently with distilled water for three times to completely remove the residues of enzyme and PBS, and then dried in a vacuum oven for 2 days. Finally, SEM was used to observe the surface morphology of the enzyme treated films. In order to confirm the reliability of the experiment, each type of sample was tested at least three times.

3. Results and discussion

3.1. Morphology analysis

The surface morphologies of SF/PDLLA composite films with varying ratios of SF to PDLLA were observed using scanning electron microscopy (Fig. 1). Fig. S1(A-I) corresponds to SEM images of SF/PDLLA composite films with different SF/PDLLA ratios at a small magnification (5 μm bar), while Fig. 1(a-i) correspond to their respective film at large magnification (100 nm bar). For the SEM images with small magnification

(Fig. S1, A-I), all the composite films showed uniformity and compatibility on the macroscopic scale. Specifically, the surface of the pure SF film (SP5-0) has a dense porous structure (Fig. 1A), while pure PDLLA (SP0-5) shows a uniform and smooth surface morphology (Fig. S1I). Once SF and PDLLA are mixed (SP5-1-SP1-5), the even surface morphology becomes rougher. Because of the differences in the two materials, there is local unevenness in heat transfer and diffusion during volatilization of the solvent [52–55], leading to local difference in surface roughness. More details about the surface morphology of the composite films are revealed by the large magnification images (Fig. 1, a-i). Specifically, the pure SF film (Fig. 1a) presents a dense nanosphereaggregation morphology [56]. In contrast, the pure PDLLA sample (Fig. 1i) shows a compact nanoparticle agglomerate structure. With the addition of PDLLA, samples SP5-1 and SP5-2 presented a uniform strip topology (Fig. 1, b-c); with further addition of PDLLA (SP5-3, SP5-5), the surface of the composite films showed the strip-like morphology of nanoparticle bulges (Fig. 1, d-e). When PDLLA becomes the dominant polymer in the composite (SP3-5), a uniform nano-spherical aggregation structure forms (Fig. 1f). At higher ratios of PDLLA (SP2-5 and SP1-5), there is a more uniform size and a denser distribution of nanospherical particles.

3.2. FTIR analysis

FTIR can be used to provide insight to the secondary protein structures related to material properties in protein-based materials. Fig. 2a shows the FTIR normalization curves of all SF/PDLLA blended films used to determine the different functional groups in the samples by

comparing peak widths and peak intensities. For SF, in general, the infrared spectral region between 1700 and 1600 cm⁻¹ is the most commonly used region for quantitative analysis of protein secondary structure [57-59]. The pure SF film (Fig. 2a, SP5-0) has three main characteristic peaks, which are located around 1643 cm⁻¹ (amide I; mainly from the C=O stretching vibrations), 1527 cm⁻¹ (amide II; the C—N stretching and the N—H in-plane bending vibrations), and 1236 cm⁻¹ (amide III; associated with the N—H bending vibrations), respectively. In addition, there is a characteristic peak of SF in the range of 3400-3250 cm⁻¹, which was related to the amine peak (N-H plane bending vibration). The peak at 2950 cm^{-1} is located in the 3000-2850cm⁻¹ alkane region, which is related to the ionic liquid BMIMCl [60]. Stanton et al. [60] studied the effects of different types of imidazolebased ionic liquids on SF/cellulose composite films and pointed out the characteristic peak in the range of 3000–2850 cm⁻¹ in the alkane region originating from the ionic liquid. The position and intensity of the peak changes with the type of ionic liquid due to the different cationic functional groups in different imidazole-based ionic liquids. In addition, the characteristic peaks of BMIMCL also include 1560 cm⁻¹ and 1158 cm⁻¹, which correspond to the C=C and C-N stretching vibrations in the imidazole ring of the ionic liquid, respectively. However, in Fig. 2a, these two peaks were not observed in the composite films. The lack of these peaks in the IR data confirms that the ionic liquid was removed after the use of the coagulant ethanol. For pure PDLLA (Fig. 2a, SP0-5), strong infrared absorption bands were shown at 3496 cm⁻¹, 2943 cm⁻¹, 1762 cm⁻¹, 1456 cm⁻¹, 1380 cm⁻¹, and 1087 cm⁻¹. These peaks are related to —OH stretching vibration, C—H stretching vibration, C=O stretching vibration, C-H bending vibration and C-O symmetric

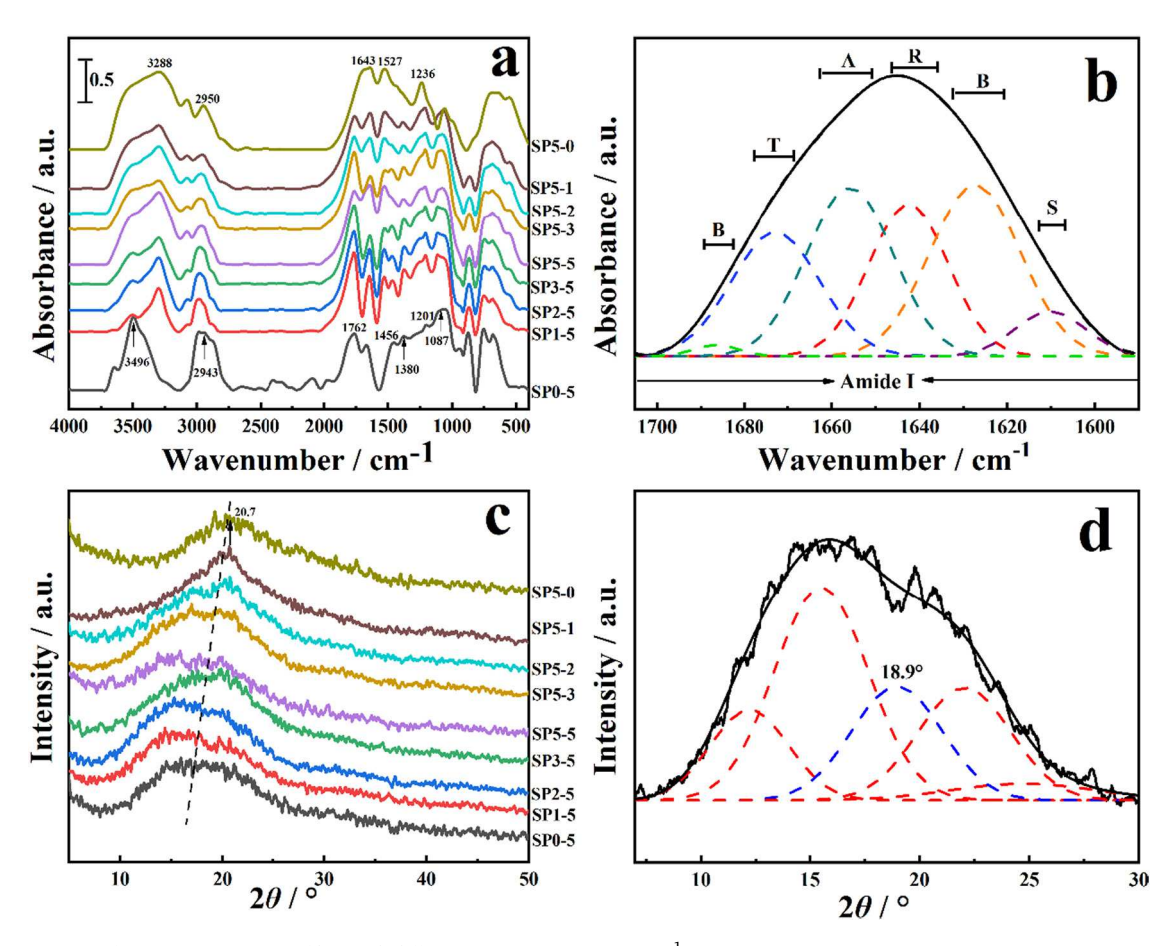


Fig. 2. (a) FTIR spectra of SF/PDLLA composite films with different ratios at 4000– 400 cm⁻¹: SF/= 5/0 (SP5-0), 5/1 (SP5-1), 5/2 (SP5-2), 5/3 (SP5-3), 5/5 (SP5-5), 3/5 (SP3-5), 2/5 (SP2-5), 1/5 (SP1-5), 0/5 (SP0-5). (b) A curve fitting example for the sample SP1-5 in the amide I region (1590– 1710 cm⁻¹); The secondary structure of the sample includes β-sheets (B), random coils (R), α-helices (A), turns (T), and side chains (S). (c) XRD spectra of all composite films with different ratios. (d) A XRD curve fitting example from sample SP1-5 in the diffraction range of 7° – 32° .

stretching vibration, respectively [61-63].

By comparing the FTIR curve of composite films (Fig. 2a), it was shown that with the increase of PDLLA content, the intensity of the absorption peaks 1643 cm⁻¹, 1527 cm⁻¹ attributed to SF gradually decreased, while the intensity of the absorption peaks 3496 cm⁻¹, 2943 cm⁻¹, 1762 cm⁻¹ related to PDLLA gradually increased. In addition, when the two-phase components were blended, many absorption peaks from individual component were shifted or changed. Specifically, the peak width of the absorption peak at 3288 cm⁻¹ is significantly smaller, and the absorption peak at 1236 cm⁻¹ shifts to 1201 cm⁻¹. The change of peak value and intensity indicates the change of material composition, further confirming interactions can occur between SF and PDLLA molecules during the solution mixing process. Similar interactions have been confirmed in previous studies [26], including in a SF/water insoluble-polyurethane composite system [64]. SF has also shown to interact with other biomolecules in composite systems. Wang et al. [65] found that because SF molecules contains active groups such as amino, hydroxyl and amide groups, interactions are possible with sodium alginate (SA) molecules that contain hydroxyl, carboxyl and other polar groups, making it easy to form different kinds of hydrogen bonds in SF/ SA composites. Additionally, different mass ratios of composites will lead to different hydrogen bond strengths, which will ultimately affect the crystallinity, thermal stability, and mechanical properties of the materials. Freddi et al. [66] believed that the addition of polyacrylamide would destroy part of the hydrogen bonds involving amide groups in SF to form new intermolecular hydrogen bonds, and thus affect the structure and mechanical properties of the composite films. It has also been found [67] that when graphene interacts with SF, strong hydrophobichydrophobic interactions, polar-polar interactions and cross-linking will occur at the two-phase interface, resulting in a compact nanolayer polymer composite. This is essential for mechanical reinforcement. In this current work, PDLLA has electron-withdrawing carbonyl (C=O) and hydrophobic hydrocarbon (-R) groups. On the one hand, the amide group (R—NH) of SF and the carbonyl group (C=O) of PDLLA will produce hydrogen bonding; on the other hand, the side chain carboxyl group (-COOH) of the residues of negatively charged amino acids (glutamic acid and aspartic acid) in SF may have electrostatic interaction with the negatively charged carbonyl group (C=O). In addition, the hydrophobic-hydrophobic interaction between the hydrophobic amino acids (such as tryptophan) of SF and the hydrophobic chains may also exist in the composite films.

During the formation of the secondary structure of SF, the interaction of polypeptide chains is mainly based on the H-bonds formed between amino groups (NH) and carbonyl groups (CO) [68]. The amide I region provides information about the stretching vibration of the C=O bond in the protein backbone. Therefore, this region was used for the study of the intermolecular and intramolecular interactions occurring in the protein chain backbone [69]. The peak fitting calculations were carried out for the amide I region from 1590 cm⁻¹ to 1710 cm⁻¹, and the content of secondary protein structures obtained is shown in Table 1. Fig. 2b shows an example of curve fitting sample using SP1-5 spectrum in the amide I region (1590–1710 cm⁻¹). The secondary structure of the sample includes β -sheets (B), random coils (R), α -helices (A), turns (T), and side chains (S). From Table 1, it can be seen side chain content had little difference between blended films. β -turns had a slightly higher difference of 6.33%, and β -sheets even higher with 15.55% difference in content between the film SP1-5 with the least β -sheets and the film SP5-0 (pure silk) with the most β -sheets. Random coil and alpha helix content both increased slightly with an increase of PDLLA content. Specifically, the β -sheet content of sample SP5-0 (pure silk) was 43.76% and the content sum of random coils and α -helices was 33.16%. With the increase of PDLLA content in the composite materials, the content sum of random coils and α -helices increased from 33.16% to 46.86%, while the content of β -sheets decreased from 43.76% to 28.21% (SP1-5). Regardless, the composite films still maintained a certain amount of β -sheet content in the film [70]. Dubey et al. [71] found that the β -sheet

Table 1Infrared fitting results of SF/PDLLA composite films in the amide I region.

Sample	β-sheet (B)/%	a-Helix + random coils(A	Side chain (S)/ %	Turn (T)/%	Silk amorphous in sample/	Amorphous in sample/%
		+ R)/%				
SP5-0	43.76 ^I / 42.23 ^X	33.16 ^I	5.87 ^I	17.21 ^I	56.24 ^I	56.24
SP5-1	39.25 ^I / 40.19 ^X	34.10 ^I	3.11 ^I	23.54 ^I	50.63 ^I	60.75
SP5-2	37.62 ^I / 36.98 ^X	35.64 ^I	3.83 ^I	22.91 ^I	44.56 ^I	62.38
SP5-3	35.58 ^I / 35.59 ^X	36.87 ^I	4.87 ^I	22.68 ^I	40.26 ^I	64.42
SP5-5	32.95 ^I / 32.18 [×]	40.71 ^I	4.73 ^I	21.61 ^I	33.53 ^I	67.05
SP3-5	30.39 ^I / 29.86 ^X	43.73 ^I	5.05 ^I	20.83 ^I	26.10 ^I	69.61
SP2-5	28.27 ^I / 27.53 [×]	46.38 ^I	4.76 ^I	20.59 ^I	20.49 ^I	71.73
SP1-5	28.21 ^I / 27.36 ^X	46.86 ^I	5.56 ^I	19.37 ^I	11.97 ^I	71.79
SP0-5	N/A	N/A	N/A	N/A	N/A	100

The superscripts I and X represent the fitting results of FTIR and XRD, respectively. All numbers have an error bar within $\pm 2\%$.

structure plays a decisive role in the thermal stability and high mechanical strength of the material. Therefore, stable β -sheet structure is of great significance for maintaining the mechanical integrity of the protein-synthetic polymer network [72]. Some studies [26-27,70] suggested that the amide group (R-NH) on SF would interact with the carbonyl group (C=O) on the molecular chain of PDLLA to form new intermolecular hydrogen bonds, resulting in the breaking of intramolecular hydrogen bonds in SF, decreasing the content of β -sheets in the material. Taddei et al. [73] believed that protonated aspartic acid (Asp) and glutamic acid (Glu) residues could act as hydrogen bond donors, and hydrogen bonds rearrangement occurs between poly (L-lactic acid) (PLLA) and SF, but this does not exclude the possibility of participation of other SF side chain groups. The formation of PLA-SF hydrogen bonds has also been reported in other previous studies [26,74–77]. In addition, with the increase of PDLLA content, the non-crystalline content of the SF component in the entire composite film decreased from 56.24% (SP5-0) to 11.97% (SP1-5), but the total amorphous content (from both SF and PDLLA) increased from 56.24% (SP5-0) to 71.79% (SP1-5).

3.3. XRD analysis

The crystal structure of SF macromolecules was analyzed by XRD data. SF is a macromolecular chain with partial repeating sequence of crystalline regions and disordered non-crystalline regions. This structure pattern leads to low crystal diffraction peaks, accompanied by broad peaks attributed to disordered regions [78]. Fig. 2c shows the XRD patterns of SF/PDLLA blended films with different proportions. It is generally believed that silkworm SF has two crystalline structures, namely silk I and silk II structures. The main conformation of Silk I structure is ordered α -helix and coils, whose corresponding diffraction angles 2θ is around 12.2° , 19.7° , 24.7° and 28.2° . The main diffraction peaks of the Silk II structure (the main conformation is β -sheets) are around 18.9° , 20.7° and 24.0° [79–80]. It can be seen from Fig. 2c that the XRD spectrum of pure PDLLA (SP0-5) shows a wide peak composition in a disordered region, indicating that the PDLLA film is almost entirely amorphous material. Except for pure PDLLA (SP0-5), all samples contain two characteristic structures from Silk I and Silk II with a wide and large diffraction peak in the diffraction range of 10.0°-25.0°. In this range, the diffraction peaks of samples SP5-0, SP5-1, and SP5-2 are located at 20.7°, corresponding to the Silk II structure. With the

increase of PDLLA content, the diffraction peak positions of SP1-5, SP2-5, SP3-5, SP5-5, and SP5-3 were significantly shifted compared with samples SP5-0, SP5-1, and SP5-2 and the diffraction peak at 20.7° gradually disappeared. That is, as the proportion of PDLLA content in the composite material increases, the β -sheet content in SF also decreases. In addition, relevant XRD curves of the composite film samples were selected for peak fitting according to the diffraction angles corresponding to Silk I and Silk II structures. Fig. 2d shows an example of curve fitting for sample SP1-5 at a diffraction angle of 7° -32°. The β -sheet content in each composite film was calculated and found to be comparable with the FTIR results (Table 1). The XRD results once again confirmed that the increase of PDLLA content would reduce the β -sheet content of SF molecules in the composite material, but still retain a certain content. For example, the β -sheet content of SP5-0 decreased from 42.23% to 27.36% (SP1-5), but the amorphous/non-crystalline content of the composite film gradually increased.

3.4. DSC analysis

DSC is one of the most important techniques to obtain evidence of miscibility of polymer-protein composites by studying the glass transition temperature (T_g) region of the composites [81]. As shown in Fig. 3a, the thermal performance of the composites was first studied by standard DSC. Meanwhile, the reversible thermal properties of the SF/PDLLA sample were measured with TMDSC. TMDSC can eliminate irreversible thermal phenomena of the samples such as water evaporation or

physical aging/degradation (Fig. 3b). It can be seen from Fig. 3a that during the heating process, the SF/PDLLA composite films of differing SF/PDLLA ratios undergo three main processes: glass transition, solvent evaporation, and thermal decomposition. Specifically, all composite films underwent glass transition in the range of 30-70 °C, which was related to the composition of PDLLA in the composites. Pure SF film (SP5-0) and all composite films showed an endothermic solvent evaporation peak between 70 °C and 180 °C [82–83]. This is mainly because SF is hydrophilic and easily absorbs water; during heating, SF will experience the evaporation of free and bound water. As a result, an endothermic peak which scales in intensity with SF content appears in the DSC thermograms. The endothermic peak of pure SF SP5-0 at 290.41 °C is mainly attributed to the decomposition of SF, while the small upward exothermic peak in this same region is caused by carbonization during decomposition [84]. The degradation peak of pure PDLLA (SP0-5) was around 315.08 °C. These thermal behaviors in the pure silk (SP5-0) and pure PDLLA (SP0-5) films were also exhibited in all the composite films. After 250 °C, there was an endothermic peak accompanied by a small exothermic peak, and the degradation peak temperature changed with the content of PDLLA in the composite materials, which may be related to the difference in the apparent morphology and β -sheet content of the composite materials. Standard differential scanning calorimetry (DSC) results show that SF and PDLLA were well blended without macroscopic phase separation.

Fig. 3b shows the reversible heat capacity curves of the samples between and 20 $^{\circ}\text{C}$ and 220 $^{\circ}\text{C}.$ It can be observed that the glass

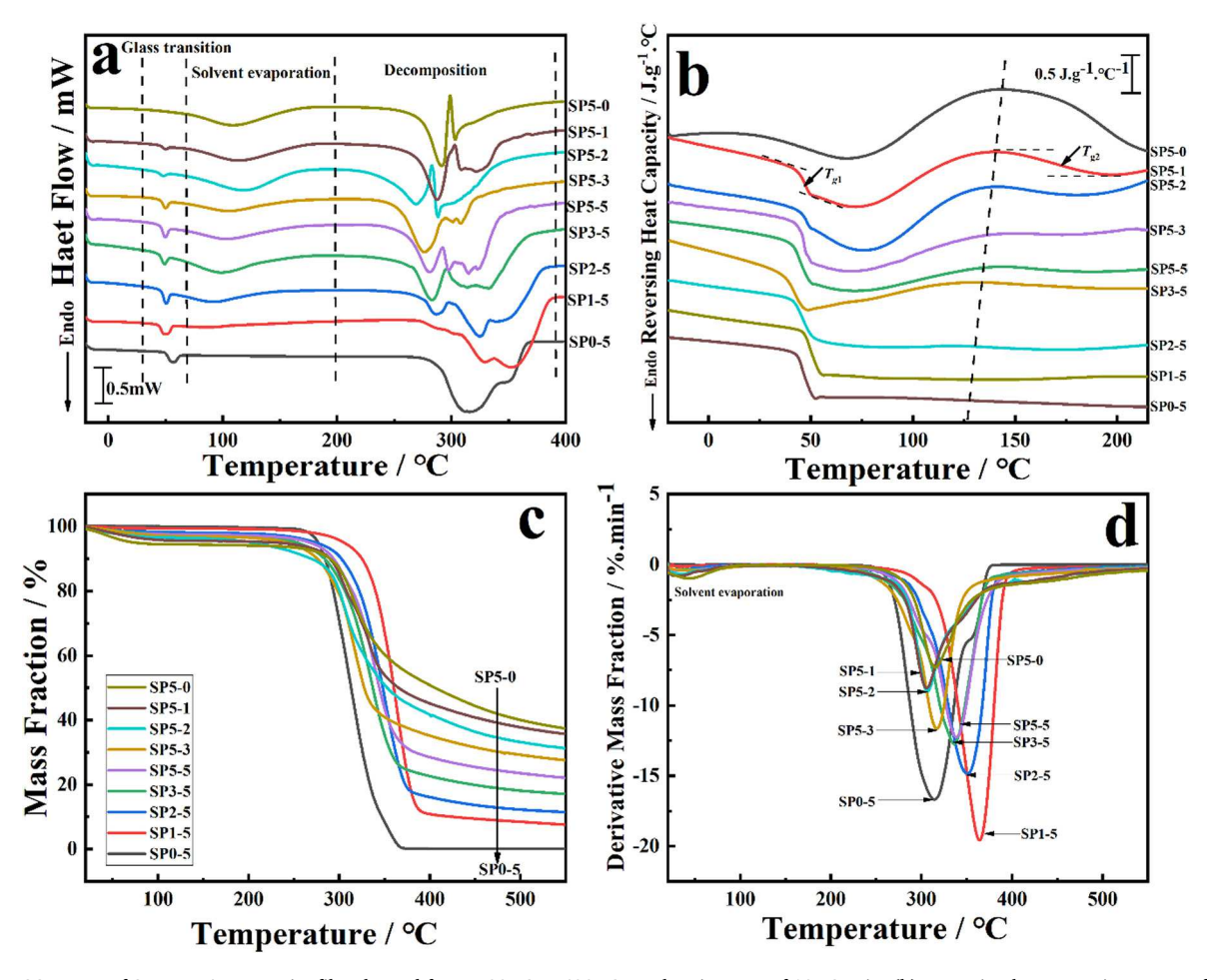


Fig. 3. (a) DSC curves of SF/PDLLA composite films heated from $-20\,^{\circ}$ C to $400\,^{\circ}$ C at a heating rate of $10\,^{\circ}$ C/min; (b) Reversing heat capacity curves of SF/PDLLA composite films were measured at heating rate of $2\,^{\circ}$ C/min using TMDSC mode, in which SF/PDLLA = 5/0(SP5-0), 5/1 (SP5-1), 5/2 (SP5-2), 5/3 (SP5-3), 5/5 (SP5-5), 3/5 (SP3-5), 2/5 (SP2-5), 1/5 (SP1-5), 0/5 (SP0-5). And (c) TG curves of all SF/PDLLA composite films heated from room temperature to $550\,^{\circ}$ C at a heating rate of $10\,^{\circ}$ C/min, respectively; (d) the first derivative of the mass percentage curve.

transition temperature of pure SF (SP5-0) appears at 186.3 °C, which is higher than that of SF films prepared from traditional aqueous solutions (about 178 °C). Some studies [85] showed that in samples treated with methanol, there was crystallization of β -sheets, which reduces the reversing heat capacity step (ΔC_p) and moves T_g to higher temperatures; similar results are seen in this study. Pure PDLLA (SP0-5) has an obvious glass transition (T_{g1}) at about 50.4 °C. For composite materials (SP5-1–SP1-5), the glass transition temperatures all appear in the temperature range of 40–50 °C and 100–200 °C for T_{g1} and T_{g2} , respectively. As the proportion of PDLLA in the composites increases, The $T_{\rm g1}$ temperature attributable to PDLLA in the range of 40-50 °C shifts slightly, moving from 45.3 °C (SP5-1) to 50.4 °C (SP0-5). Ho et al. [86] found that the $T_{\rm g}$ peak of silk fiber/PLA composites also shifted slightly to a lower temperature compared to pure PLA. Tao et al. [87] explained that this phenomenon is due to the ionic or hydrogen bond interactions between the soft and the hard segments of the polymer blend, which enhances the microphase separation, leading to a decrease in the T_g of the soft segment of the composite film. Meanwhile, the glass transition contributed by the SF component greatly shifted to lower temperatures, from 186.3 °C (SP5-0) to 140.2 °C (SP1-5). It can be seen from the above DSC results that SF strongly interacts with PDLLA. In particular, adding a small amount of silk proteins into the PDLLA matrix (e.g., SP1-5) can greatly improve the miscibility of the blend, making the individual T_{g} s of silk and PDLLA much closer to each other. However, the two characteristic glass transitions on the TMDSC curves also indicate a potential microphase separation of the two components, although the large shift of the two T_2 s indicates that the macrophases of the two separate components have been well fused during the blending process (this is also supported by the SEM images in Fig. 1 and Fig. S1) [88-93]. Liu et al. [94] pointed out that morphology and structure are important factors affecting the glass transition temperature when studying styreneisoprene star block copolymers. Different chemical and physical crosslinking interactions between the two polymers in different proportions would lead to different branched chain lengths and branched degrees, and ultimately lead to different phase separation degrees. At the same time, some literature [95] suggested when using DSC to study block copolymers that if the flexible chain of one polymer component is mixed in another polymer, its glass transition temperature would be reduced. Therefore, in this study, compared with the pure SF and pure PDLLA samples, the glass transition temperatures related to SF and PDLLA in the composite films were both lower. In addition, it can be seen from Table 2 that the specific heat capacity ΔC_{p1} at the glass transition temperature related to PDLLA increased from 0.142 $\rm J \cdot g^{-1} \cdot ^{\circ} C^{-1}$ (SP5-1) to 0.602 J·g⁻¹.°C⁻¹ (SP0-5). And the specific heat capacity $\Delta C_{\rm n2}$ at the glass transition temperature related to SF decreased from 0.095 $J \cdot g^{-1} \cdot {}^{\circ}C^{-1}$ (SP5-0) to 0.013 $J \cdot g^{-1} \cdot {}^{\circ}C^{-1}$ (SP1-5), which again confirmed the results of FTIR and XRD. FTIR and XRD results showed that with the continuous addition of PDLLA, the SF-related amorphous content

Table 2The glass transition temperature and the corresponding change in heat capacity during the glass transition of SF/PDLLA composite films with different proportions.

Sample	$T_{\rm g1}/^{\circ}{\rm C}$	$\Delta C_{\rm p1}/{ m J}\cdot{ m g}^{-1}\cdot{ m ^{\circ}}{ m C}^{-1}$	$T_{\rm g2}/^{\circ}{\rm C}$	$\Delta C_{p2}/J \cdot g^{-1} \cdot \circ C^{-1}$
SP5-0	N/A	N/A	186.3	0.095
SP5-1	45.3	0.142	168.9	0.083
SP5-2	45.4	0.222	158.6	0.063
SP5-3	45.6	0.262	157.2	0.052
SP5-5	46.0	0.286	156.7	0.043
SP3-5	46.3	0.328	154.3	0.028
SP2-5	46.7	0.376	143.5	0.020
SP1-5	46.8	0.476	140.2	0.013
SP0-5	50.4	0.602	N/A	N/A

 $T_{\rm g}$ and $\Delta C_{\rm p}$ are the glass transition temperature and the corresponding change in heat capacity during the glass transition, respectively. All numbers have an error bar within $\pm 5\%$.

(related to $\Delta C_{\rm p2}$) in the composite samples decreased from 56.24% to 11.97%, but the total amorphous content (related to sum of $\Delta C_{\rm p1}$ and $\Delta C_{\rm p2}$) increased from 56.24% (SP5-0) to 100% (SP0-5) (Table 1). All these phenomena imply interactions and thermodynamic compatibility between SF and PDLLA.

3.5. TG analysis

Thermogravimetric analysis (TG) technology plays an important role in studying the thermal stability and thermal decomposition of materials (Fig. 3). It can be used to evaluate the thermal stability of the material, including the initial decomposition temperature (T_{onset}), the temperature corresponding to the maximum decomposition rate (T_P) , the total weight loss rate and other characteristics. The thermogravimetric curves of different composite films obtained by thermogravimetric analysis (TGA) are shown in Fig. 3c. Fig. 3d shows the first derivative plot of the mass percentage curve, which helps better determine the critical thermal stability temperatures shown in the composite material. It can be seen from Fig. 3c that during the initial heating process between room temperature and 200 °C, the weight loss of all samples was within 10%. The maximum loss of pure SF (SP5-0) during this initial heating process is 5.88% because SF has good hydrophilicity and hygroscopicity, making it more susceptible to the dehydration process. During this process, bound and free water are released from the sample [96], corresponding to the solvent evaporation peak appearing in the first derivative of mass loss thermogram. In this temperature range, there is almost no mass loss of pure PDLLA, with only 0.37% mass loss. The thermal weight loss process of all SF/PDLLA composites mainly occurs between 200 °C and 400 °C, and there was only one obvious weight loss step, which showed that the decomposition process of SF/PDLLA composites was completed in one step, indicating that the two components of SF and PDLLA had good thermodynamic compatibility. In this stage, the mass loss of all composite samples was rapid, which is mainly related to the fracture of the molecular backbone and the decomposition of molecular domains in the composite polymer [97]. Interestingly, for the sample SP1-5, the mass loss (about 0.81% at 200 °C) was less than that of sample SP2-5 and SP3-5 (about 2.23% and 3.08%). Once the initial decomposition temperature was reached, the mass of sample SP1-5 decreased significantly, and its decomposition rate was faster, reaching about 19.57%/min. Therefore, the composition of the composites will significantly affect the initial decomposition temperature and thermal degradation rate of the sample (Fig. 3c, d).

The $T_{\rm onset}$, $T_{\rm p}$ and total weight loss percentage of the samples at 550 °C are listed in Table 3 (Fig. S2). When the initial decomposition temperature $T_{\rm onset}$ and the maximum decomposition rate of pure SF and pure PDLLA films are observed, the thermal stability of SF films is significantly better than that of pure PDLLA films. The $T_{\rm onset}$ of all SF/

Table 3 TG thermal decomposition data of SF/PDLLA composite films with different mass ratios at a heating rate of 10 $^{\circ}\text{C/min},$ and the water contact angle of samples.

Sample	T _{onset} ∕ °C	<i>T</i> _p /°C	Weight Loss at 550 $^{\circ}$ C/ $^{\circ}$	Water contact angle/
SP5-0	292.64	315.79	62.61	66.73°
SP5-1	287.23	305.75	64.32	68.52°
SP5-2	288.51	306.48	68.77	70.94
SP5-3	288.68	316.79	72.45	72.76
SP5-5	306.48	338.78	77.90	73.48
SP3-5	303.84	336.02	82.91	74.32
SP2-5	318.80	350.59	88.56	76.51
SP1-5	335.21	364.45	92.43	83.68
SP0-5	282.52	314.01	99.89	87.97

 $T_{
m onset}$ represents the initial decomposition temperature of the sample; $T_{
m p}$ represents the temperature corresponding to the maximum decomposition rate of the sample; wt. Loss represents the percentage of mass remaining when the sample is heated to 550 °C.

PDLLA composite films are also higher than that of pure PDLLA films, indicating that the SF component can improve the thermal stability of the composites. Interestingly, with the continuous addition of PDLLA, the initial decomposition temperature T_{onset} generally shifts to higher temperatures for the composite samples, increasing from 287.23 °C (SP5-1) to 335.21 °C (SP1-5), indicating that the thermal stability of the composites could be improved by adding a certain amount of PDLLA compared with pure SF film. This is mainly because there is a close molecular interaction between SF and PDLLA, and there could be a strong intermolecular hydrogen bonding interaction between the -NH of SF and the C=O group on the PDLLA chain, thus improving the thermal stability of the composite films. On the contrary, with the increase of SF content, the content of β -sheets in the composites increases, and this change of the material structure will affect its physical properties. Therefore, the glass transition temperature of the composites also increases [85]. However, due to the high-water content of SF and its easy decomposition, the thermal stability of composites was not improved by the increase of SF content [70]. In the main degradation stage, the mass loss of all samples was rapid and the maximum decomposition rate gradually increased with the increase of PDLLA content. This was observed as an increase in T_p from 305.75 °C (SP5-1) to 364.45 °C (SP1-5), indicating that the SF component could slow down the decomposition rate of the composites at higher temperature. As the content of PDLLA increases, the residual amount at 550 °C also decreases. For example, the residual mass in sample SP5-0 is about 37.39%, while the sample SP0-5 has only about 0.11% residual mass at 550 $^{\circ}$ C. It has been reported [98] that above 450 °C, the residues in the composites are mainly carbon generated by the carbonization of SF under nitrogen atmosphere, and the residual amount increases with the increase of the SF content, which is consistent with the experimental results. At the same time, these results also illustrate the good miscibility of the two materials.

3.6. Hydrophilicity analysis

The static water contact angle of the material surface is an important indicators for evaluating the hydrophilicity/hydrophobicity of the material [99-100]. The surface properties of the material (i.e., chemical composition, hydrophilicity and hydrophobicity, roughness, porosity) determine its performance and applications. In this study, the water contact angles of SF-PDLLA composite films with mass ratios of 5:0, 5:2, 5:5, 2:5, and 0:5 were 66.73°, 70.94°, 73.48°, 76.51°, and 87.97°, respectively (Fig. 4a, Table 3, Fig. S3). Among them, the pure SF film (SP5-0) has the lowest static water contact angle, indicating that SF has good hydrophilicity. However, the pure PDLLA (SP0-5) has the highest static water contact angle and high hydrophobicity, which is due to the rich hydrophobic ester bonds in its molecular backbone and the lack of hydrophilic groups [101–102]. When the PDLLA component increases, the water contact angle of the composite film also increases, which means the hydrophilic/hydrophobic properties of the material can be adjusted by changing the content of PDLLA. On the contrary, with the increase of SF content, the water contact angle of the composite film gradually decreases, which shows that the increase of SF content is beneficial to improving the hydrophilicity of the composite film. For ideal tissue engineering material, in addition to having certain mechanical properties, good plasticity, and biodegradability, the most important point is that it must have good biocompatibility. To accomplish this, a good material-cell interface is necessary. High hydrophilicity is more conducive to cell adhesion, growth, and proliferation [12], but the hydrophobic surface is more conducive to protein absorption [73] which may be necessary for certain growth factors and extracellular proteins.

3.7. Biocompatibility analysis

Mouse fibroblasts (L929) were then used for in vitro cytotoxicity

experiments to evaluate the biocompatibility and cell viability of SF/ PDLLA composite films. Fig. 4b shows the survival rate of mouse fibroblasts cultured on SF/PDLLA composite films with different mass ratios (SP5-0, SP5-1, SP5-2, SP5-3, SP5-5, SP3-5, SP2-5, SP1-5, and SP0-5) at 6, 24 and 48 h of culture time. With the increase of culture time, the cell activity of all the composite films showed an increasing trend. Specifically, the cell viability of sample SP3-5 cultured for 6, 24, and 48 h was 101.9%, 104.7%, and 107.1%, respectively. After 24 h of culture, the composite film containing SF has higher cell activity than pure PDLLA film, indicating that the cell viability of the sample was related to the SF content. The cell viability of the samples with high SF content (SP5/1, SP5/2) was significantly better than that of the samples with low SF content (SP1/5, SP2/5, SP3/5, SP5/5, SP5/3). For example, when the mass ratio of SF to PDLLA was 5:2 and 5:1, the cell viability was relatively high at 111.7% and 114.4%, respectively, which was close to that of the pure SF film (118.9%). In addition, after 48 h of cell proliferation, it showed the same pattern as the result of 24 h of culture. In summary, the presence of SF in the SF/PDLLA composite film contributes to the ability of cell adhesion and growth. It has been reported [73] that a more favorable microenvironment was found on the surface of SF/PLA composite nanofibers than pure PLA. The improved proliferation on the surface of SF/PLA composite nanofibers may be attributed to the interaction between SF and cells. SF is a protein polymer with repeating hydrophobic-hydrophilic amino acid units [23,30-31,35,52], which can provide a mild and indolent place for cell adhesion and differentiation [26,73]. Meinel et al. [103] found that in vitro cell proliferation on silk films can be enhanced compared to collagen and tissue culture plates. Wray et al. [104] believed that the difference in cell viability may be related to the way proteins were adsorbed to the surface of the silk film and the difference in the distribution of surface charge during the fabrication of the silk film. Other biocompatibility experiments in vivo and in vitro have also proved similar cell characteristics [36,73,103,105]. In this blend, the hydrophilicity of SF gives it the ability to interact with the negatively charged surface of the cell. While PDLLA has poor hydrophilicity and lacks biological activity and cell affinity. Therefore, in SF/PDLLA composite films, the hydrophilicity is significantly improved compared to pure PDLLA.

3.8. Enzymatic degradation

To verify the crystalline and amorphous structure in the SF/PDLLA composite films, SEM was used to observe the structural change of blend samples treated in a chymotrypsin/PBS buffer solution for 24 h (Fig. 4c). Chymotrypsin is a proteolytic enzyme secreted by the pancreas, which can only degrade the amorphous region of silk and PDLLA polymer materials to obtain a highly crystalline material structure [106-109]. For pure SF (SP5-0), a relatively flat shape with a few cracks was observed, indicating that the SF film is dominated by β -sheet crystals through ethanol and heat treatments during the fabrication process. The poly(D,L-lactic acid) material used in this study is a completely amorphous polymer. Therefore, for SP5-2, SP5-5 and SP3-5 samples, micropores appeared after enzymolysis for 24 h. The quantity and size of the micropores gradually increased with the increase of PDLLA content. This indicates that the PDLLA domain and amorphous domain of SF have been combined to form micelle structures, and the β -sheet crystals of SF have formed a cross-linked network in the SF/PDLLA films. After being digested by chymotrypsin, the amorphous micelle structures in the films became holes, and the crystal domain formed a scaffold-like structure.

This structure also provided us with a clearer picture of the microphase separation behavior discussed in the DSC study: when the silk content is small, protein molecules are not able to form a cross-linked network, therefore, the temperature difference between $T_{\rm g1}$ and $T_{\rm g2}$ (Table 2) is small, indicating that the blends are almost completely fused at the molecular level without obvious microphase separation; once the silk content increases, the formation of a scaffold-like crystal network promotes the microphase separation, resulting in a greater temperature

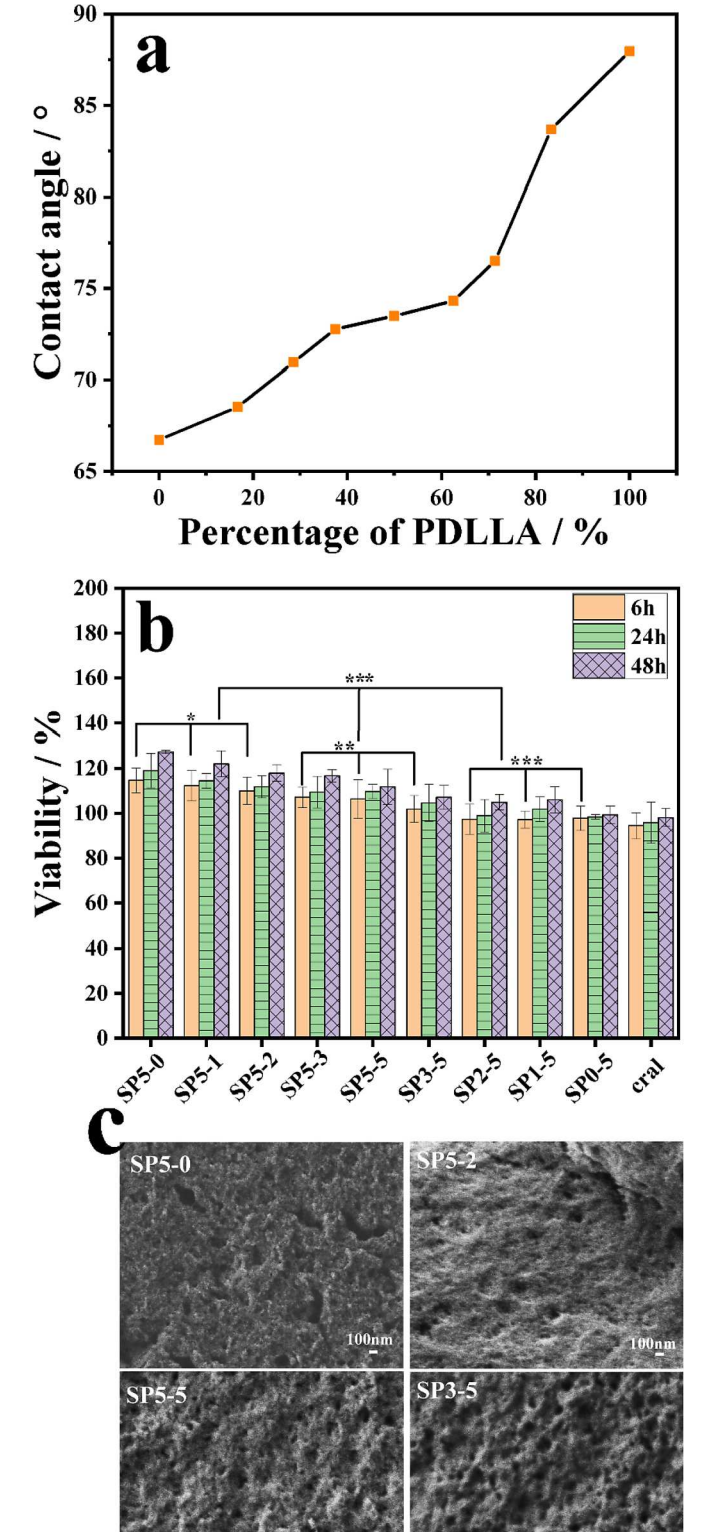


Fig. 4. (a)Water contact angle of SF/PDLLA composite films with different mass ratios, where SF/ PDLLA = 5/0 (SP5-0), 5/2 (SP5-2), 5/5 (SP5-5), 2/5 (SP2-5), 0/5 (SP0-5). And (b) MTT assay method was used to determine the survival rate of mouse fibroblasts cultured on different mass ratios of SF/PDLLA composite films for 6 h, 24 h, and 48 h. The number of equivalent cells on the well plate $(1 \times 10^4/\text{well})$ was used as the control value (* $p \le 0.1$, ** $p \le 0.01$, *** $p \le 0.001$, $p \ge 0.001$,

films (SP5-0, SP5-2, SP5-5 and SP3-5) after chymotrypsin enzymatic degradation for $24\ h.$

difference between the two T_g s in the DSC curve.

3.9. Self-assembly mechanism in the binary solvent system

The final properties of the blends generally depend on the compatibility between the individual polymers [93,110-111]. Therefore, the acquisition of a compatible system of proteins (SF) and synthetic polymers (PDLLA) is an important goal in this polymer blend system. According to the classical thermodynamics and kinetics of polymer blending theory, it can be found that there are three main types of miscibility based on polymer blends. One is a completely miscible mixture (one phase). The second is semi-miscible at microscale, in which one polymer can be partially dissolved into another at the molecular level, and small polymer chains are evenly distributed across the main polymer network. The third is immiscible blends, in which the two polymers are completely immiscible with phase separation. Compatible blends refer to blends that exhibit good properties regardless of whether it is miscible (one-phase), semi-miscible, or immiscible (macrophase separation) blends. Miscible and partially miscible mixtures in thermodynamic miscibility can produce homogeneous properties on a macroscopic scale, while immiscible blends may process heterogeneous properties due to the uneven properties of different parts of the material

Silk fibroin is mainly composed of H-chain (391 kDa), L-chain (28 kDa) and glycoprotein chain P25 (25 kDa) to form regular crystalline regions (about 2/3) and amorphous area (about 1/3) [114-115]. The crystalline region, mainly consisting of glycine (Gly), alanine (Ala) and serine (Ser), is evenly distributed in the continuous amorphous region, mainly containing phenylalanine (Phe), tyrosine (Tyr) and tryptophan (Try) [29,116–117]. Generally, the dissolution of SF in ionic liquid is believed to be a process that the anions such as halogen, carboxylic acid, and acetic acid in ionic liquid interact with the hydroxyl groups in SF to destroy its intermolecular and intramolecular hydrogen bonds [118–119]. Simultaneously, the synergistic effect of nucleophilicity, electrophilicity and charge polarity of anions and cations will also accelerate the destruction of hydrogen bonds between β -sheet crystalline structures, and finally achieve dissolution, in which SF presents mainly random coils and α -helix structures [96,120]. After being treated with organic solvents [121] or high temperatures [122], or by physical shearing [123], recrystallization of silk fibroin can occur [100]. When SF is blended with amorphous PDLLA with electron-withdrawing carbonyl group (C=O) and hydrophobic hydrocarbon group (-R), hydrophobic-hydrophobic interactions can be induced between the molecular chains [65–67] besides their hydrogen bonding interactions. These interactions can promote self-assembly of molecular chains in SF/ PDLLA blends to form micelle structures [124–125]. Hydrogen bonding and static electrostatic interaction were mainly driven by enthalpy, while hydrophobic-hydrophobic interaction was driven by entropy [126-128]. Although the microphase separation properties (for example, two glass transitions in DSC) were shown thermodynamically, the strong interaction between polymer chains will overcome the effect of microphase separation to maintain a thermodynamically miscible system at the macroscale level. In this case, samples can still show a homogeneous morphology on the macroscale and provide satisfactory homogeneous properties for the material. Our observations indicate that SF/PDLLA blends have established strong interactions with improved physical and biological properties compared to the pure polymers.

Therefore, based on the above results, a self-assembly model for this protein-synthetic polymer material is proposed (Fig. 5). SF is first dissolved into ionic liquid, forming a non-crystalline structure (Fig. 5a), with both uncrystallizable blocks and crystallizable blocks. Subsequently, it is mixed with amorphous PDLLA (Fig. 5b) to obtain a

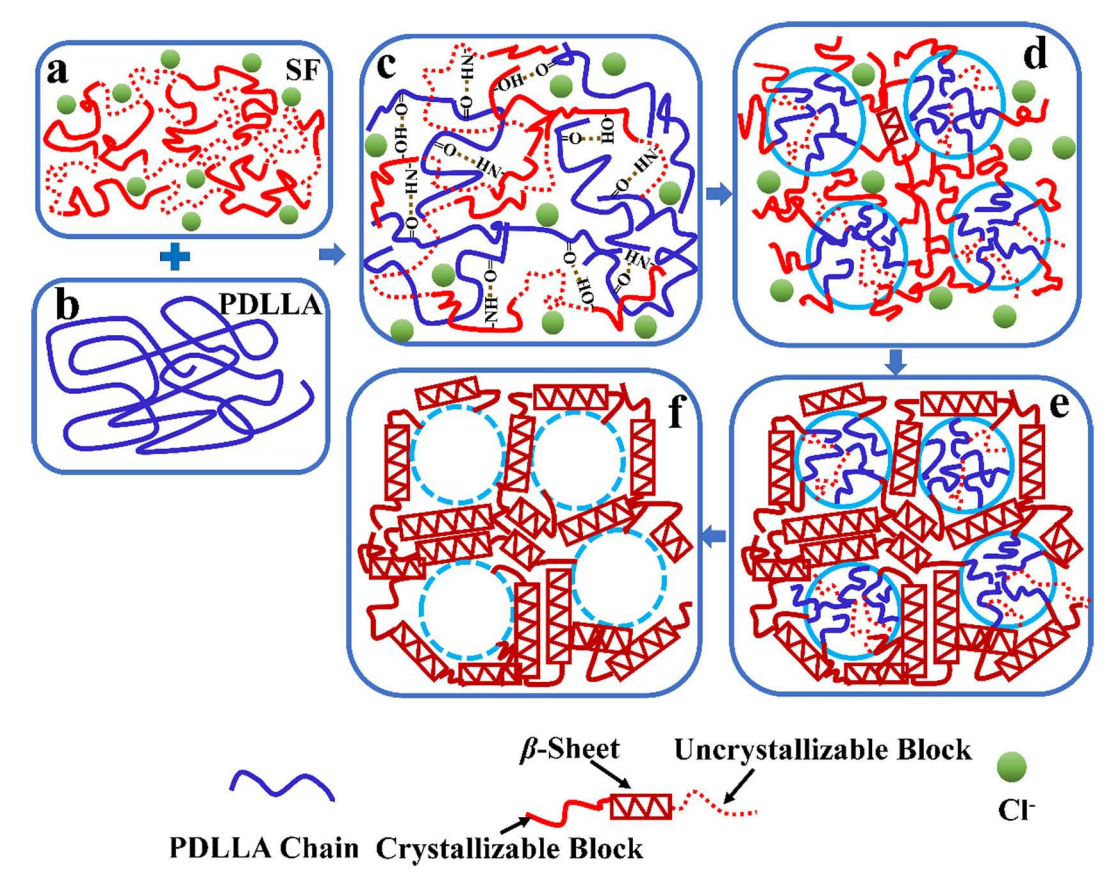


Fig. 5. Schematic diagram of the dissolution and regeneration process of SF/PDLLA films. (a) SF is dissolved in ionic liquid to form a non-crystalline structure; (b) PDLLA dissolved in DMF to form an amorphous structure; (c) through blending, the molecular chains of SF and PDLLA undergo hydrogen bonding, hydrophobic-hydrophobic interactions, and electrostatic interactions; (d) during heating and refluxing, the composites self-assemble into micellar structures, due to the microphase separation between the non-crystallizable and crystallizable domains; (e) through ethanol washing and drying, β-sheet crystals are induced, and form a crosslinked network that wraps the micelle structures. (f) After enzymatic biodegradation, the amorphous micelles are biodegraded and appear as micropores on the SF/PDLLA films.

macroscopically homogeneous blend solution (Fig. 5c). After being heated to 95 °C with reflux, more micelle-like precursor structures are formed, mainly due to the hydrogen bonding and hydrophobic-hydrophobic interactions. After heating and drying, microphase separation occurs between crystallizable and uncrystallizable domains (Fig. 5d). Through ethanol treatment and deionized water washing, the anions in the composite films are removed and β -sheet crystals are formed [83,126–127], located in the crystallizable domain (Fig. 5e). These physical crosslinks can help promote the formation of micelle structures within the crystal network [128–129]. After 24 h enzymatic biodegradation, the amorphous micelles are biodegraded and appear as micropores on the SF/PDLLA films (Fig. 5f). The morphology of micelles can be further controlled by changing the mixing ratio of SF and PDLLA, as shown in the SEM images of Fig. 1 and Fig. 4c [130].

4. Conclusion

In this study, different mass ratios of SF/PDLLA composite materials were prepared by using an ionic liquid 1-butyl-3-methylimidazolium chloride (BMIMCl) and *N*,*N*-dimethylformamide (DMF) binary solvent system. The morphology, structure, thermal properties, and biological properties of composites were systematically studied. The results show that SF and PDLLA are miscible in this solvent system. By simply changing the mass ratio of SF and PDLLA and physical blending methods, the morphology, structure, physical, and biological properties of SF/PDLLA composite materials can be tuned. The self-assembly mechanism of the SF/PDLLA composite film are discussed, which is of great significance for revealing the self-assembly principle of the SF/

PDLLA composite films. On this basis, the structure-property relationship of protein-synthetic polymer composites can be well established, which can provide guidance for the fabrication of high-performance biopolymer-based materials. For example, one potential application of these materials is to embed drugs into the hydrophobic chain segments of the structure through hydrophobic-hydrophilic, electrostatic, or noncovalent metal ion interactions. This allows for a controlled release of the drugs at the site of action. In addition, with the help of the hydrophilic segment, the interaction between the bioactive molecules and the composite materials can be enhanced, promoting the process of tissue regeneration. Therefore, this protein-synthetic polymer system can play an important role in drug delivery and regenerative medicine in the future

CRediT authorship contribution statement

Qianqian Deng: Conceptualization, Methodology, Investigation, Formal analysis, Data curation, Writing – original draft, Validation, Writing – review & editing. Fang Wang: Conceptualization, Methodology, Investigation, Formal analysis, Data curation, Writing – original draft, Validation, Writing – review & editing. Christopher R. Gough: Formal analysis, Data curation, Writing – original draft, Validation, Writing – review & editing. Xiao Hu: Formal analysis, Data curation, Writing – original draft, Validation, Writing – review & editing.

Declaration of competing interest

The authors declare that they have no known competing financial

interests or personal relationships that could have appeared to influence the work reported in this paper.

Acknowledgements

This study is supported by the National Natural Science Foundation of China (21973045). C.R.G. and X.H. are supported by Rowan University Seed Research Grants and the US NSF Biomaterials Program (DMR-1809541).

Appendix A. Supplementary data

Supplementary data to this article can be found online at https://doi.org/10.1016/j.ijbiomac.2021.12.060.

References

- [1] D.L. Tian, T. Li, R.C. Zhang, Q. Wu, T.H. Chen, P.C. Sun, A. Ramamoorthy, Conformations and intermolecular interactions in cellulose/silk fibroin blend films: a solid-state NMR perspective, J. Phys. Chem. B. 121 (25) (2017) 6108–6116, https://doi.org/10.1021/acs.jpcb.7b02838.
- [2] S. Feroz, N. Muhammad, J. Ranayake, G. Dias, Keratin based materials for biomedical applications, Bioact. Mater. 5 (3) (2020) 496–509, https://doi.org/ 10.1016/j.bioactmat.2020.04.007.
- [3] S. Liu, Y.Y. Xie, L.D. Wang, C.X. Tai, D. Chen, D. Mu, Y.Y. Cui, B. Wang, A multichannel collagen scaffold loaded with neural stem cells for the repair of spinal cord injury, Neural Regen. Res. 16 (11) (2021) 2284–2292, https://doi.org/ 10.4103/1673-5374.310698.
- [4] B.T. Tomoda, F.G. Corazza, M.M. Beppu, P.S. Lopes, M.A. de Moraes, Silk fibroin membranes with self-assembled globular structures for controlled drug release, J. Appl. Polym. Sci. 137 (16) (2020) 48763, https://doi.org/10.1002/app.48763.
- [5] X.T. Jia, C.Y. Wang, C. Zhao, Y. Ge, G.G. Wallace, Toward biodegradable Mg-Air bioelectric batteries composed of silk fibroin-polypyrrole film, Adv. Funct. Mater. 26 (9) (2016) 1454–1462, https://doi.org/10.1002/adfm.201503498.
 [6] B.L. Wang, H.Y. Li, Q.Y. Yao, Y.L. Zhang, X.D. Zhu, T.L. Xia, J. Wang, G. Li, X.
- [6] B.L. Wang, H.Y. Li, Q.Y. Yao, Y.L. Zhang, X.D. Zhu, T.L. Xia, J. Wang, G. Li, X. G. Li, S.L. Ni, Local in vitro delivery of rapamycin from electrospun PEO/PDLLA nanofibers for glioblastoma treatment, Biomed. Pharmacother. 83 (2016) 1345–1352, https://doi.org/10.1016/j.biopha.2016.08.033.
- [7] Y.C. Cui, R.H. Jin, Y. Zhou, M.R. Yu, Y. Ling, L.Q. Wang, Crystallization enhanced thermal-sensitive hydrogels of PCL-PEG-PCL triblock copolymer for 3D printing, Biomed. Mater. 16 (3) (2021), 035006, https://doi.org/10.1088/1748-605X/ abc38e
- [8] A. Gao, Q. Yang, L.X. Xue, Poly (l-lactic acid)/silk fibroin composite membranes with improved crystallinity and thermal stability from non-solvent induced phase separation processes involving hexafluoroisopropanol, Compos. Sci. Technol. 132 (2016) 38–46, https://doi.org/10.1016/j.compscitech.2016.06.011.
- [9] K. Guiza, R.Ben Affi, K. Mougin, C. Vaulot, L. Michelin, L. Josien, G. Schrodj, A. Ghorbal, Development of novel and ecological keratin/cellulose-based composites for absorption of oils and organic solvents, Environ. Sci. Pollut. Res. 28 (34) (2021) 46655–46668, https://doi.org/10.1007/s11356-020-11260-7.
- [10] Q.C. Liu, F. Wang, Y.Y. Li, H.Y. Yu, Q.Y. Ma, Z.G. Gu, Comparative studies of structure, thermal decomposition mechanism and thermodynamic parameters of two kinds of silk fibroin films, Sci. Sin. Chim. 49 (7) (2019) 1014–1029, https:// doi.org/10.1360/N032018-00265.
- [11] S. Park, Y. Oh, J. Yun, E. Yoo, D. Jung, K.S. Park, K.K. Oh, S.H. Lee, Characterization of blended cellulose/biopolymer films prepared using ionic liquid, Cellulose 27 (9) (2020) 5101–5119, https://doi.org/10.1007/s10570-020-03152-3
- [12] K.Y. Cai, K.D. Yao, S.B. Lin, Z.M. Yang, X.Q. Li, H.Q. Xie, T.W. Qing, L.B. Gao, Poly (D, L-lactic acid) surfaces modified by silk fibroin: effects on the culture of osteoblast in vitro, Biomaterials 23 (4) (2002) 1153–1160, https://doi.org/ 10.1016/S0142-9612(01)00230-7.
- [13] J.M. Chen, H. Venkatesan, J.L. Hu, Chemically modified silk proteins, Adv. Eng. Mater. 20 (7) (2018) 1700961, https://doi.org/10.1002/adem.201700961.
- [14] F. Wang, H. Liu, Y.Y. Li, Y.J. Li, Q.Y. Ma, J. Zhang, X. Hu, Tunable biodegradable polylactide silk fibroin scaffolds fabricated by a solvent-free pressure-controllable foaming technology, ACS. Appl. Bio. Mater. 3 (12) (2020) 8795–8807, https://doi.org/10.1021/acsabm.0c01157.
- [15] M.Y. Yang, Silk-based biomaterials, Microsc. Res. Tech. 80 (3) (2017) 269–271, https://doi.org/10.1002/jemt.22846.
- [16] A. Salama, Cellulose/silk fibroin assisted calcium phosphate growth: novel biocomposite for dye adsorption, Int. J. Biol. Macromol. 165 (2020) 1970–1977, https://doi.org/10.1016/j.ijbiomac.2020.10.074.
- [17] C. Zhang, X. Chen, Z.Z. Shao, Sol-gel transition of regenerated silk fibroins in ionic Liquid/Water mixtures, ACS Biomater. Sci. Eng. 2 (1) (2016) 12–18, https://doi.org/10.1021/acsbiomaterials.5b00149.
- [18] K.A. Callaway, Y. Xue, V. Altimari, G.X. Jiang, X. Hu, Comparative investigation of thermal and structural behavior in renewably sourced composite films of eveneven nylons (610 and 1010) with silk fibroin, Polymers 10 (9) (2018) 1029, https://doi.org/10.3390/polym10091029.

- [19] F. Zhang, R.C. Yang, P. Zhang, J.Z. Qin, Z.H. Fan, B.Q. Zuo, Water-rinsed nonmulberry silk film for potential tissue engineering applications, Acs Omega 4 (2) (2019) 3114–3121, https://doi.org/10.1021/acsomega.8b03542.
- [20] Q.C. Liu, F. Wang, Z.G. Gu, Q.Y. Ma, X. Hu, Exploring the structural transformation mechanism of chinese and Thailand silk fibroin fibers and formicacid fabricated silk films, Int. J. Mol. Sci. 19 (11) (2018) 3309, https://doi.org/ 10/3300/fibre10113309
- [21] G.S. Perrone, G.G. Leisk, T.J. Lo, J.E. Moreau, D.S. Haas, B.J. Papenburg, E. B. Golden, B.P. Partlow, S.E. Fox, A.M.S. Ibrahim, S.J. Lin, D.L. Kaplan, The use of silk-based devices for fracture fixation, Nat. Commun. 5 (2014) 3385, https://doi.org/10.1038/ncomms4385.
- [22] S. Bai, S. Liu, C. Zhang, W. Xu, Q. Lu, H. Han, D.L. Kaplan, H. Zhu, Controllable transition of silk fibroin nanostructures: an insight into in vitro silk self-assembly process, Acta Biomater. 9 (8) (2013) 7806–7813, https://doi.org/10.1016/j. actbio 2013.04.033
- [23] C. Holland, A.E. Terry, D. Porter, F. Vollrath, Natural and unnatural silks, Polymer 48 (12) (2007) 3388–3392, https://doi.org/10.1016/j. polymer.2007.04.019.
- [24] N.M. Siqueira, K.C. Garcia, R. Bussamara, F.S. Both, M.H. Vainstein, R.M. D. Soares, Poly (lactic acid)/chitosan fiber mats: investigation of effects of the support on lipase immobilization, Int. J. Biol. Macromol. 72 (2015) 998–1004, https://doi.org/10.1016/j.ijbiomac.2014.08.048.
- [25] Y.P. Jiao, F.Z. Cui, Surface modification of polyester biomaterials for tissue engineering, Biomed. Mater. 2 (4) (2007) 24–37, https://doi.org/10.1088/1748-6041/2/4/R02
- [26] F. Wang, H. Wu, V. Venkataraman, X. Hu, Silk fibroin- poly (lactic acid) biocomposites: effect of protein-synthetic polymer interactions and miscibility on material properties and biological responses, Mater. Sci. Eng. C Mater. Biol. Appl. 104 (2019), 109890, https://doi.org/10.1016/j.msec.2019.109890.
- [27] M. Tesfaye, R. Patwa, A. Gupta, M.J. Kashyap, V. Katiyar, Recycling of poly (lactic acid)/silk based bionanocomposites films and its influence on thermal stability, crystallization kinetics, solution and melt rheology, Int. J. Biol. Macromol. 101 (2017) 580–594, https://doi.org/10.1016/j. ijbiomac.2017.03.085.
- [28] D.K. Ma, G. An, M. Liang, Y.G. Liu, B. Zhang, Y.S. Wang, A composited PEG-silk hydrogel combining with polymeric particles delivering rhBMP-2 for bone regeneration, Mater. Sci. Eng. C Mater. Biol. Appl. 65 (2016) 221–231, https://doi.org/10.1016/j.msec.2016.04.043.
- [29] G.H. Altman, F. Diaz, C. Jakuba, T. Calabro, R.L. Horan, J.S. Chen, H. Lu, J. Richmond, D.L. Kaplan, Silk-based biomaterials, Biomaterials 24 (3) (2003) 401–416, https://doi.org/10.1016/S0142-9612(02)00353-8.
- [30] S. Gomes, I.B. Leonor, J.F. Mano, R.L. Reis, D.L. Kaplan, Silk-based biomaterials, Microsc. Res. Tech. (2012) 75–92, https://doi.org/10.1002/9783527652273. ch4.
- [31] J.G. Hardy, L.M. Romer, T.R. Scheibel, Polymeric materials based on silk proteins, Polymer 49 (20) (2008) 4309–4327, https://doi.org/10.1016/j. polymer.2008.08.006.
- [32] B.D. Lawrence, M. Cronin-Golomb, I. Georgakoudi, D.L. Kaplan, F.G. Omenetto, Bioactive silk protein biomaterial Systems for Optical Devices, Biomacromolecules 9 (4) (2008) 1214–1220.
- [33] M.Z. Li, W. Tao, S.Z. Lu, S. Kuga, Compliant film of regenerated Antheraea pernyi silk fibroin by chemical crosslinking, Int. J. Biol. Macromol. 32 (3–5) (2003) 159–163, https://doi.org/10.1016/S0141-8130(03)00049-7.
 [34] I.C. Um, H.Y. Kweon, Y.H. Park, S. Hudson, Structural characteristics and
- [34] I.C. Um, H.Y. Kweon, Y.H. Park, S. Hudson, Structural characteristics and properties of the regenerated silk fibroin prepared from formic acid, Int. J. Biol. Macromol. 29 (2) (2001) 91–97.
- [35] X. Chen, D.P. Knight, Z.Z. Shao, F. Vollrath, Regenerated bombyx silk solutions studied with rheometry and FTIR, Polymer 42 (25) (2001) 09969–09974, https://doi.org/10.1016/S0032-3861(01)00541-9.
- [36] B.W. Thimm, S. Wust, S. Hofmann, H. Hagenmuller, R. Muller, Initial cell precultivation can maximize ECM mineralization by human mesenchymal stem cells on silk fibroin scaffolds, Acta Biomater. 7 (5) (2011) 2218–2228, https://doi.org/ 10.1016/i.actbio.2011.02.004.
- [37] D.M. Phillips, L.F. Drummy, D.G. Conrady, D.M. Fox, R.R. Naik, M.O. Stone, P. C. Trulove, H.C. De Long, R.A. Mantz, Dissolution and regeneration of Bombyx mori silk fibroin using ionic liquids, J. Am. Chem. Soc. 126 (44) (2004) 14350–14351, https://doi.org/10.1021/ja046079f.
- [38] M. Kostag, K. Jedvert, O.A. El Seoud, Engineering of sustainable biomaterial composites from cellulose and silk fibroin: fundamentals and applications, Int. J. Biol. Macromol. 167 (2021) 687–718, https://doi.org/10.1016/j. ijbiomac.2020.11.151.
- [39] A.E. Visser, R.P. Swatloski, W.M. Reichert, R. Mayton, S. Sheff, A. Wierzbicki, J. H. Davis, R.D. Rogers, Task-specific ionic liquids for the extraction of metal ions from aqueous solutions, Chem. Commun. 01 (2001) 135–136, https://doi.org/10.1039/B008041L.
- [40] Q. Wang, Q. Chen, Y.H. Yang, Z.Z. Shao, Effect of various dissolution systems on the molecular weight of regenerated silk fibroin, Biomacromolecules 14 (1) (2013) 285–289, https://doi.org/10.1021/bm301741q.
- [41] Q. Wang, Y.H. Yang, X. Chen, Z.Z. Shao, Investigation of rheological properties and conformation of silk fibroin in the solution of AmimCl, Biomacromolecules 13 (6) (2012) 1875–1881, https://doi.org/10.1021/bm300387z.
- [42] A. Fournier, G. de Robillard, J. Bousfiha, M.S. Ahmed, C.H. Devillers, J. Andrieu, An electrochemical process to prepare and recycle biobased ionic liquids, Green Chem. 21 (23) (2019) 6290–6298, https://doi.org/10.1039/c9gc02055a.

- [43] J. Lu, A. He, S.Y. Li, L.R. Nie, W. Zhang, S. Yao, Synthesis, purification and recycling of ionic liquid, Mini. Rev. Org. Chem. 12 (5) (2015) 435–448, https://doi.org/10.2174/1570193X13666151125230810.
- [44] S. Keskin, D. Kayrak-Talay, U. Akman, O. Hortacsu, A review of ionic liquids towards supercritical fluid applications, J. Supercrit. Fluids 43 (1) (2007) 150–180, https://doi.org/10.1016/j.supflu.2007.05.013.
- [45] S.J. Zhang, J.J. Wang, X.M. Lu, Q. Zhou, Structures and interactions of ionic liquids, Struct. Bond. 151 (2014), https://doi.org/10.1007/978-3-642-38619-0.
- [46] S.J. Zhang, N. Sun, X.Z. He, X.M. Lu, X.P. Zhang, Physical properties of ionic liquids: database and evaluation, J. Phys. Chem. Ref. Data 35 (4) (2006) 1475–1517, https://doi.org/10.1063/1.2204959.
- [47] R.D. Rogers, K.R. Seddon, Ionic liquids-solvents of the future, Science 302 (5646) (2003) 792–793, https://doi.org/10.1126/science.1090313.
- [48] S.A. Love, E. Popov, K. Rybacki, X. Hu, D. Salas-de la Cruz, Facile treatment to fine-tune cellulose crystals in cellulose-silk biocomposites through hydrogen peroxide, Int. J. Biol. Macromol. 147 (2020) 569–575, https://doi.org/10.1016/j. iibiomac.2020.01.100.
- [49] A. Ghosh, S. Clerens, S. Deb-Choudhury, J.M. Dyer, Thermal effects of ionic liquid dissolution on the structures and properties of regenerated wool keratin, Polym. Degrad. Stab. 108 (2014) 108–115, https://doi.org/10.1016/j.polymdegradstab.
- [50] A. Ota, R. Beyer, U. Hageroth, A. Muller, P. Tomasic, F. Hermanutz, M. R. Buchmeiser, Chitin/cellulose blend fibers prepared by wet and dry-wet spinning, Polym. Adv. Technol. 32 (1) (2021) 335–342, https://doi.org/10.1002/ pat 5080
- [51] M.G. Fuster, G. Carissimi, M.G. Montalban, G. Villora, Improving anticancer therapy with naringenin-loaded silk fibroin nanoparticles, Nanomaterials 10 (4) (2020) 718, https://doi.org/10.3390/nano10040718.
- [52] C.Z. Zhou, F. Confalonieri, M. Jacquet, R. Perasso, Z.G. Li, J. Janin, Silk fibroin: structural implications of a remarkable amino acid sequence, Proteins 44 (2) (2001) 119–122, https://doi.org/10.1002/prot.1078.
- [53] Y.F. Huang, K. Bailey, S. Wang, X.S. Feng, Silk fibroin films for potential applications in controlled release, React. Funct. Polym. 116 (2017) 57–68, https://doi.org/10.1016/j.reactfunctpolym.2017.05.007.
- [54] A. Reizabal, D.M. Correia, C.M. Costa, L. Perez-Alvarez, J.L. Vilas-Vilela, S. Lanceros-Mendez, Silk fibroin bending actuators as an approach toward natural polymer based active materials, ACS Appl. Mater. Interfaces 11 (33) (2019) 30197–30206, https://doi.org/10.1021/acsami.9b07533.
- [55] S.S. Silva, T.C. Santos, M.T. Cerqueira, A.P. Marques, L.L. Reys, T.H. Silva, S. G. Caridade, J.F. Mano, R.L. Reis, The use of ionic liquids in the processing of chitosan/silk hydrogels for biomedical applications, Green Chem. 14 (5) (2012) 1463–1470. https://doi.org/10.1039/C2GC16535.J.
- [56] F. Wang, H.Y. Yu, Z.G. Gu, L. Si, Q.C. Liu, X. Hu, Impact of calcium chloride concentration on structure and thermal property of thai silk fibroin films, J. Therm. Anal. Calorim. 130 (2) (2017) 851–859, https://doi.org/10.1007/ s10973-017-6388-z.
- [57] X. Hu, Q. Lu, L. Sun, P. Cebe, X.Q. Wang, X.H. Zhang, D.L. Kaplan, Biomaterials from ultrasonication-induced silk fibroin hyaluronic acid hydrogels, Biomacromolecules 11 (11) (2010) 3178–3188, https://doi.org/10.1021/ bm1010504.
- [58] J. Zhang, R. Rajkhowa, J.L. Li, X.Y. Liu, X.G. Wang, Silkworm cocoon as natural material and structure for thermal insulation, Mater. Des. 49 (2013) 842–849, https://doi.org/10.1016/j.matdes.2013.02.006.
- [59] Y. Xue, F. Wang, M. Torculas, S. Lofland, X. Hu, Formic acid regenerated Mori, tussah, eri, thai, and muga silk materials: mechanism of self-assembly, ACS Biomater. Sci. Eng. 5 (12) (2019) 6361–6373, https://doi.org/10.1021/acchiomaterials.ph/05177
- [60] J. Stanton, Y. Xue, P. Pandher, L. Malek, T. Brown, X. Hu, D. Salas-de la Cruz, Impact of ionic liquid type on the structure, morphology and properties of silkcellulose biocomposite materials, Int. J. Biol. Macromol. 108 (2018) 333–341, https://doi.org/10.1016/j.ijbiomac.2017.11.137.
- [61] B.B. Wang, H.M. Lou, H.L. Xu, J.P. Zhao, Q.J. Wang, Q. Shi, Y.H. Deng, High voltage, solvent-free solid polymer electrolyte based on a star-comb PDLLA-PEG copolymer for lithium ion batteries, RSC Adv. 8 (12) (2018) 6373–6380, https:// doi.org/10.1039/C7RA13664A.
- [62] H.T. Zou, C.H. Yi, L.X. Wang, H.T. Liu, W.L. Xu, Thermal degradation of poly (lactic acid) measured by thermogravimetry coupled to Fourier transform infrared spectroscopy, J. Therm. Anal. Calorim. 97 (3) (2009) 929–935, https://doi.org/10.1007/s10973-009-0121-5.
- [63] J.J. Ahire, D. Robertson, D.P. Neveling, A.J. Van Reenen, L.M.T. Dicks, Hyaluronic acid-coated poly (D, L-lactide) (PDLLA) nanofibers prepared by electrospinning and coating, RSC Adv. 6 (41) (2016) 34791–34796, https://doi org/10.1039/C6RA01996J.
- [64] X.Y. Liu, C.C. Zhang, W.L. Xu, H.T. Liu, C.X. Ouyang, Blend films of silk fibroin and water-insoluble polyurethane prepared from an ionic liquid, Mater. Lett. 65 (15–16) (2011) 2489–2491, https://doi.org/10.1016/j.matlet.2011.05.017.
- [65] Z.Q. Wang, H.W. Yang, Z. Zhu, Study on the blends of silk fibroin and sodium alginate: hydrogen bond formation, structure and properties, Polymer 163 (2019) 144–153, https://doi.org/10.1016/j.polymer.2019.01.004.
- [66] G. Freddi, M. Tsukada, S. Beretta, Structure and physical properties of silk fibroin/polyacrylamide blend films, J. Appl. Polym. Sci. 71 (10) (1999) 1563–1571, https://doi.org/10.1002/(SICI)1097-4628(19990307)71:10% 3C1563::AID-APP4%3E3.0.CO;2-E.
- [67] F. Wang, S.S.J. Aravind, H. Wu, J. Forys, V. Venkataraman, K. Ramanujachary, X. Hu, Tunable green graphene-silk biomaterials: mechanism of protein-based

- nanocomposites, Mater. Sci. Eng. C Mater. Biol. Appl. 79 (2017) 728–739, https://doi.org/10.1016/j.msec.2017.05.120.
- [68] M.D. Chomachayi, A. Jalali-Arani, F.R. Beltran, M.U. de la Orden, Biodegradable nanocomposites developed from PLA/PCL blends and silk fibroin nanoparticles: study on the microstructure, thermal behavior, crystallinity and performance, J. Polym. Environ. 28 (4) (2020) 1252–1264, https://doi.org/10.1007/s10924-020.01684.0
- [69] M. McGill, G.P. Holland, D.L. Kaplan, Experimental methods for characterizing the secondary structure and thermal properties of silk proteins, Macromol. Rapid Commun. 40 (1) (2019) 1800390, https://doi.org/10.1002/marc.201800390.
- [70] F. Wang, Y.Y. Li, C.R. Gough, Q.C. Liu, X. Hu, Dual-crystallizable silk fibroin/poly (L-lactic Acid) biocomposite films: effect of polymer phases on protein structures in protein-polymer blends, Int. J. Mol. Sci. 22 (4) (2021) 1871, https://doi.org/ 10.3390/ijms22041871.
- [71] P. Dubey, S. Murab, S. Karmakar, P.K. Chowdhury, S. Ghosh, Modulation of self-assembly process of fibroin: an insight for regulating the conformation of silk biomaterials, Biomacromolecules 16 (12) (2015) 3936–3944, https://doi.org/10.1021/acs.biomac.5b01258.
- [72] T.Y. Zhong, Z.J. Jiang, P. Wang, S.Y. Bie, F. Zhang, B.Q. Zuo, Silk fibroin/ copolymer composite hydrogels for the controlled and sustained release of hydrophobic/hydrophilic drugs, Int. J. Pharm. 494 (1) (2015) 264–270, https:// doi.org/10.1016/j.ijpharm.2015.08.035.
- [73] P. Taddei, S. Tozzi, G. Zuccheri, S. Martinotti, E. Ranzato, V. Chiono, I. Carmagnola, M. Tsukada, Intermolecular interactions between B.Mori silk fibroin and poly(L-lactic acid) in electrospun composite nanofibrous scaffolds, Mater. Sci. Eng. C Mater. Biol. Appl. 70 (2017) 777–787, https://doi.org/ 10.1016/j.msec.2016.09.055.
- [74] S.J. Ling, L. Zhou, W. Zhou, Z.Z. Shao, X. Chen, Conformation transition kinetics and spinnability of regenerated silk fibroin with glycol, glycerol and polyethylene glycol, Mater. Lett. 81 (2012) 13–15, https://doi.org/10.1016/j. matlet.2012.04.136.
- [75] T. Furukawa, H. Sato, R. Murakami, J.M. Zhang, I. Noda, S. Ochiai, Y. Ozaki, Raman micro spectroscopy study of structure, dispersibility, and crystallinity of poly(hydroxybutyrate)/poly(L-lactic acid) blends, Polymer 47 (9) 3132-3140. doi:10.1016/j.polymer.2006.03.010.
- [76] G. Kister, G. Cassanas, M. Vert, B. Pauvert, A. Terol, Vibrational analysis of Poly (L-lactic acid), J. Raman Spectrosc. 26 (4) (1995) 307–311, https://doi.org/ 10.1002/jrs.1250260409.
- [77] R.P. Wool, R.S. Bretzlaff, B.Y. Li, C.H. Wang, R.H. Boyd, Infrared and raman spectroscopy of stressed polyethylene, J. Polym. Sci. Part B Polym. Phys. 24 (1986) 1039–1066, https://doi.org/10.1002/polb.1986.090240508.
- [78] A. Reizabal, C.M. Costa, P.G. Saiz, B. Gonzalez, L. Perez-Alvarez, R.F. de Luis, A. Garcia, J.L. Vilas-Vilela, S. Lanceros-Mendez, Processing strategies to obtain highly porous silk fibroin structures with tailored microstructure and molecular characteristics and their applicability in water remediation, J. Hazard. Mater. 403 (2021), 123675, https://doi.org/10.1016/j.jhazmat.2020.123675.
- [79] R.C. Yang, P. Wu, X.H. Wang, Z.K. Liu, C. Zhang, Y.L. Shi, F. Zhang, B.Q. Zuo, A novel method to prepare tussah/Bombyx mori silk fibroin-based films, RSC Adv. 8 (39) (2018) 22069–22077, https://doi.org/10.1039/C8RA03266A.
- [80] Z.H. Fan, L.Y. Xiao, G.H. Lu, Z.H. Ding, Q. Lu, Water-insoluble amorphous silk fibroin scaffolds from aqueous solutions, J. Biomed. Mater. Res. B, Appl. Biomater. 108 (3) (2020) 798–808, https://doi.org/10.1002/jbm.b.34434.
- [81] X. Hu, P. Cebe, A.S. Weiss, F. Omenetto, D.L. Kaplan, Protein-based composite materials, Mater. Today 15 (5) (2012) 208–215, https://doi.org/10.1016/S1369-7021(12)70091-3.
- [82] X. Hu, D. Kaplan, P. Cebe, Dynamic protein-water relationships during β-sheet formation, Macromolecules 41 (11) (2008) 3939–3948, https://doi.org/10.1021/ ma071551d
- [83] A. Hadadi, J.W. Whittaker, D.E. Verrill, X. Hu, L. Larini, D. Salas-de la Cruz, A hierarchical model to understand the processing of Polysaccharides/Protein-based films in ionic liquids, Biomacromolecules 19 (10) (2018) 3970–3982, https://doi.org/10.1021/acs.biomac.8b00903.
- [84] P. Jandura, B. Riedl, B.V. Kokta, Thermal degradation behavior of cellulose fibers partially esterified with some long chain organic acids, Polym. Degrad. Stab. 70 (3) (2000) 387–394, https://doi.org/10.1016/S0141-3910(00)00132-4.
- [85] X. Hu, D. Kaplan, P. Cebe, Determining Beta sheet crystallinity in fibrous proteins by thermal analysis and infrared spectroscopy, Macromolecules 39 (18) (2006) 6161–6170, https://doi.org/10.1021/ma0610109.
- [86] M.P. Ho, H. Wang, K.T. Lau, J.S. Leng, Effect of silk fiber to the mechanical and thermal properties of its biodegradable composites, J. Appl. Polym. Sci. 127 (4) (2013) 2389–2396, https://doi.org/10.1002/app.37539.
- [87] Y.Z. Tao, Y. Yan, W.L. Xu, Physical characteristics and properties of waterborne polyurethane materials reinforced with silk fibroin powder, J. Polym. Sci. B Polym. Phys. 48 (9) (2010) 940–950, https://doi.org/10.1002/polb.21981.
- [88] R.Z. Xiao, Z.W. Zeng, G.L. Zhou, J.J. Wang, F.Z. Li, A.M. Wang, Recent advances in PEG–PLA block copolymer nanoparticles, Int. J. Nanomedicine 5 (2010) 1057–1065, https://doi.org/10.2147/ijn.S14912.
- [89] A.C. Shi, Frustration in block copolymer assemblies, J. Phys.:Condens. Matter. 33 (25) (2021), 253001, https://doi.org/10.1088/1361-648X/abf8d0.
- [90] I. Akiba, K. Sakurai, Characterizing block-copolymer micelles used in nanomedicines via solution static scattering techniques, Polym. J. (2021), https://doi.org/10.1038/s41428-021-00489-9.
- [91] S.S. Jang, H.C. Moon, J. Kwak, D. Bae, Y. Lee, J.K. Kim, W.B. Lee, Phase behavior of star-shaped polystyrene-block-poly(methyl methacrylate) copolymers, Macromolecules 47 (15) (2014) 5295–5302, https://doi.org/10.1021/ ma500584x.

- [92] D. Pospiech, L. Haussler, K. Eckstein, H. Komber, D. Voigt, D. Jehnichen, P. Friedel, A. Gottwald, W. Kollig, H.R. Kricheldorf, Synthesis and phase separation behaviour of high performance multiblock copolymers, High. Perform. Polym. 13 (2) (2001) 275–292, https://doi.org/10.1088/0954-0083/13/2/324.
- [93] M.A. de Moraes, M.F. Silva, R.F. Weska, M.M. Beppu, Silk fibroin and sodium alginate blend: miscibility and physical characteristics, Mater. Sci. Eng. C Mater. Biol. Appl. 40 (2014) 85–91, https://doi.org/10.1016/j.msec.2014.03.047.
- [94] J.J. Liu, J. Wang, J.C. Sheng, The glass transition temperature and intermediate phase relaxation of star-shaped block copolymers of polystyrene and polyisoprene, Chin. J. Appl. Chem. 3 (1986) 41–45.
- [95] C.F. Chen, Y.D. Wang, Y.Q. Cheng, M.Y. Wu, The structure characterization on poly(ethylene terephthalate)-poly(tetramethylene ether) multiblock copolymer, Polym. Commun. 1 (1983) 408–413.
- [96] B. Blessing, C. Trout, A. Morales, K. Rybacki, S.A. Love, S.M. Omalley, X. Hu, D. Salas-de la Cruz, G. Lamoureux, The impact of composition and morphology on ionic conductivity of silk/cellulose bio-composites fabricated from ionic liquid and varying percentages of coagulation agents, Int. J. Mol. Sci. 21 (13) (2020) 4695, https://doi.org/10.3390/ijms21134695.
- [97] H.L. Zhu, X.X. Feng, H.P. Zhang, Y.H. Guo, J.Z. Zhang, J.Y. Chen, Structural characteristics and properties of silk fibroin/poly (lactic acid) blend films, J. Biomater. Sci. Polym. Ed. 20 (9) (2012) 1259–1274, https://doi.org/10.1163/ 156856209X452980.
- [98] S. Sheik, G.K. Nagaraja, K. Prashantha, Effect of silk fiber on the structural, thermal, and mechanical properties of PVA/PVP composite films, Polym. Eng. Sci. 58 (11) (2017) 1923–1930, https://doi.org/10.1002/pen.24801.
- [99] J.W. Qin, Y.Y. Jiang, J.J. Fu, Y.Q. Wan, R.H. Yang, W.D. Gao, H.B. Wang, Evaluation of drug release property and blood compatibility of aspirin-loaded electrospun PLA/RSF composite nanofibers, Iran. Polym. J. 22 (10) (2013) 729–737, https://doi.org/10.1007/s13726-013-0171-1.
- [100] L.L. Tian, M.P. Prabhakaran, J. Hu, M.L. Chen, F. Besenbacher, S. Ramakrishna, Coaxial electrospun poly (lactic acid)/silk fibroin nanofibers incorporated with nerve growth factor support the differentiation of neuronal stem cells, RSC Adv. 5 (62) (2015) 49838–49848, https://doi.org/10.1039/C5RA05773F.
- [101] A. Basu, K.R. Kunduru, S. Doppalapudi, A.J. Domb, W. Khan, Poly (lactic acid) based hydrogels, Adv. Drug Deliv. Rev. 107 (2016) 192–205, https://doi.org/10.1016/j.addr.2016.07.004.
- [102] R.M. Rasal, A.V. Janorkar, D.E. Hirt, Poly (lactic acid) modifications, Prog. Polym. Sci. 35 (3) (2010) 338–356, https://doi.org/10.1016/j.prognolymsci.2009.12.003.
- [103] L. Meinel, S. Hofmann, V. Karageorgiou, C. Kirker-Head, J. McCool, G. Gronowicz, L. Zichner, R. Langer, G. Vunjak-Novakovic, D.L. Kaplan, The inflammatory responses to silk films in vitro and in vivo, Biomaterials 26 (2) 147-155. doi: 10.1016/j.biomaterials.2004.02.047.
- [104] L.S. Wray, X. Hu, J. Gallego, I. Georgakoudi, F.G. Omenetto, D. Schmidt, D. L. Kaplan, Effect of processing on silk-based biomaterials: reproducibility and biocompatibility, J. Biomed. Mater. Res. B Appl. Biomater. 99 (1) (2011) 89–101, https://doi.org/10.1002/jbm.b.31875.
- [105] S.H. Jang, M.S. Oh, H.I. Baek, K.C. Ha, J.Y. Lee, Y.S. Jang, Oral Administration of Silk Peptide Enhances the maturation and cytolytic activity of natural killer cells, Immune Netw. 18 (5) (2018), https://doi.org/10.4110/in.2018.18.e37.
- [106] M.Z. Li, M. Ogiso, N. Minoura, Enzymatic degradation behavior of porous silk fibroin sheets, Biomaterials 24 (2) (2003) 357–365, https://doi.org/10.1016/ S0142-9612(02)00326-5.
- [107] X. Hu, Q. Lu, D.L. Kaplan, P. Cebe, Microphase separation controlled β -sheet crystallization kinetics in fibrous proteins, Macromolecules 42 (6) (2009) 2079–2087, https://doi.org/10.1021/ma802481p.
- [108] M.S. Reeve, S.P. McCarthy, M.J. Downey, R.A. Gross, Polylactide stereochemistry: effect on enzymatic degradability, Macromolecules 27 (3) (1994) 825–831, https://doi.org/10.1021/ma00081a030.
- [109] S.J. Sheng, X. Hu, F. Wang, Q.Y. Ma, M.F. Gu, Mechanical and thermal property characterization of poly-L-lactide (PLLA) scaffold developed using pressurecontrollable green foaming technology, Mater. Sci. Eng. C Mater. Biol. Appl. 49 (2015) 612–622, https://doi.org/10.1016/j.msec.2015.01.025.
- [110] M.S. Kumar, D.K. Bhat, Miscibility of poly (vinylidene fluoride) and cellulose acetate blends in dimethyl formamide, Asian J. Chem. 23 (4) (2011) 1474–1478.
- [111] Y.J. Kim, G.S. Shin, I.T. Lee, B.K. Kim, Miscible and immiscible blends of ABS with PMMA. I. Morphology and rheology, J. Appl. Polym. Sci. 47 (2) (1993) 295–304, https://doi.org/10.1002/app.1993.070470209.

- [112] Z.K. Marwat, M.K. Baloch, Miscibility between PS and PSAN affected by solvent and temperature of the system, Chin. J. Polym. Sci. 32 (11) (2014) 1442–1449, https://doi.org/10.1007/s10118-014-1534-6.
- [113] E. Kiran, Polymer miscibility, phase separation, morphological modifications and polymorphic transformations in dense fluids, J. Supercrit. Fluids 47 (3) (2009) 466–483, https://doi.org/10.1016/j.supflu.2008.11.010.
- [114] S. Aliramaji, A. Zamanian, M. Mozafari, Super-paramagnetic responsive silk fibroin/chitosan/magnetite scaffolds with tunable pore structures for bone tissue engineering applications, Mater. Sci. Eng. C Mater. Biol. Appl. 70 (2017) 736–744, https://doi.org/10.1016/j.msec.2016.09.039.
- [115] S. Inoue, K. Tanaka, F. Arisaka, S. Kimura, K. Ohtomo, S. Mizuno, Silk fibroin of Bombyx mori is secreted, assembling a high molecular mass elementary unit consisting of H-chain, L-chain, and P25, with a 6:6:1 molar ratio, J. Biol. Chem. 275 (51) (2000) 40517–40528, https://doi.org/10.1074/jbc.M006897200.
- [116] C.Y. Hayashi, R.V. Lewis, Evidence from flagelliform silk cDNA for the structural basis of elasticity and modular nature of spider silks, J. Mol. Biol. 275 (5) (1998) 773–784, https://doi.org/10.1006/jmbi.1997.1478.
- [117] K. Mita, S. Ichimura, T.C. James, Highly repetitive structure and its organization of the silk fibroin gene, J. Mol. Evol. 38 (6) (1994) 583–592, https://doi.org/ 10.1007/RF00175878
- [118] X.D. Yang, C.D. Qiao, Y. Li, T.D. Li, Dissolution and resourcfulization of biopolymers in ionic liquids, React. Funct. Polym. 100 (2016) 181–190, https:// doi.org/10.1016/j.reactfunctpolym.2016.01.017.
- [119] L.A. Aslanov, Ionic liquids: liquid structure, J. Mol. Liq. 162 (3) (2011) 101–104, https://doi.org/10.1016/j.molliq.2011.06.006.
- [120] C.X. Xie, W.J. Li, Q.Q. Liang, S.T. Yu, L. Li, Fabrication of robust silk fibroin film by controlling the content of β-sheet via the synergism of UV-light and ionic liquids, Appl. Surf. Sci. 492 (2019) 55–65, https://doi.org/10.1016/j. apsusc.2019.06.144.
- [121] Z.B. Cao, X. Chen, J.R. Yao, L. Huang, Z.Z. Shao, The preparation of regenerated silk fibroin microspheres, Soft Matter 3 (7) (2007) 910–915, https://doi.org/ 10.1039/B703139D.
- [122] N. Jaramillo-Quiceno, C. Alvarez-Lopez, A. Restrepo-Osorio, Structural and thermal properties of silk fibroin films obtained from cocoon and waste silk fibers as raw materials, Procedia Eng. 200 (2017) 384–388, https://doi.org/10.1016/j. proeng.2017.07.054.
- [123] H.J. Jin, D.L. Kaplan, Mechanism of silk processing in insects and spiders, Nature 424 (6952) (2003) 1057–1061, https://doi.org/10.1038/nature01809.
- [124] F.J. Jiang, K. Liu, M.H. Zhao, X.C. Tao, X. Hu, S.Z. Lu, Tunable high-molecular-weight silk fibroin polypeptide materials: fabrication and self-assembly mechanism, ACS Appl. Bio. Mater. 3 (5) (2020) 3248–3259, https://doi.org/10.1021/acsabm.0c00231...
- [125] J.Z. Wang, Y.Q. Song, P.C. Sun, Y.L. An, Z.K. Zhang, L.Q. Shi, Reversible interactions of proteins with mixed Shell polymeric micelles: tuning the surface Hydrophobic/Hydrophilic balance toward efficient artificial chaperones, Langmuir 32 (11) (2016) 2737–2749, https://doi.org/10.1021/acs.langmuir.6b00356.
- [126] Y. Chong, C.C. Ge, Z.X. Yang, J.A. Garate, Z.L. Gu, J.K. Weber, J.J. Liu, R.H. Zhou, Reduced cytotoxicity of graphene nanosheets mediated by blood-protein coating, ACS Nano 9 (6) (2015) 5713–5724, https://doi.org/10.1021/nn5066606.
- [127] A. Ibanez-Fonseca, D. Orbanic, F.J. Arias, M. Alonso, D.I. Zeugolis, J. C. Rodriguez-Cabello, Influence of the thermodynamic and kinetic control of self-assembly on the microstructure evolution of silk-elastin-like recombinamer hydrogels, Small 16 (28) (2020) 2001244, https://doi.org/10.1002/smll_202001244
- [128] T. Vu, Y. Xue, T. Vuong, M. Erbe, C. Bennet, B. Palazzo, L. Popielski, N. Rodriguez, X. Hu, Comparative study of ultrasonication-induced and naturally self-assembled silk fibroin-wool keratin hydrogel biomaterials, Int. J. Mol. Sci. 17 (9) (2016) 1497, https://doi.org/10.3390/ijms17091497.
- [129] X.H. Qu, L. Yan, S. Liu, Y.F. Tan, J. Xiao, Y. Cao, K. Chen, W.Q. Xiao, B. Li, X. L. Liao, Preparation of silk fibroin/hyaluronic acid hydrogels with enhanced mechanical performance by a combination of physical and enzymatic crosslinking, J. Biomater. Sci. Polym. Ed. 32 (12) (2021) 1635–1653, https://doi.org/10.1080/09205063.2021.1932070.
- [130] J. Jung, I.H. Lee, E. Lee, J. Park, S. Jon, PH-sensitive polymer nanospheres for use as a potential drug delivery vehicle, Biomacromolecules 8 (11) (2007) 3401–3407, https://doi.org/10.1021/bm700517z.